2013

# A three-equation bypass transition model based on the intermittency function

Xuan Ge
*Iowa State University*

**A three-equation bypass transition model based on the intermittency function**

by

Xuan Ge

A thesis submitted to the graduate faculty

in partial fulfillment of the requirements for the degree of

MASTER OF SCIENCE

Major: Aerospace Engineering

Program of Study Committee:

Paul Durbin, Major Professor

Alric Rothmayer

Lester Schmerr

Iowa State University

Ames, Iowa

2013

## DEDICATION

I would like to dedicate this thesis to my parents without whose support I would not have been able to complete this work. I would also like to thank my friends and family for their loving guidance and support.

# TABLE OF CONTENTS

# LIST OF TABLES

## LIST OF FIGURES

## ACKNOWLEDGEMENTS

I would like to take this opportunity to express my thanks to those who helped me with various aspects of conducting research and the writing of this thesis. First and foremost, Dr. Paul Durbin for his guidance, patience and support throughout this research and the writing of this thesis. His insights and talents have often inspired and encouraged me to attempt and explore. I would also like to thank my committee members for their efforts and contributions to this work: Dr. Alric Rothmayer and Dr. Lester Schmerr. I would additionally like to thank Mr. Sunil Arolla for his guidance and help throughout this work. Thanks also to Mr. John Dickerson and Mr. Jim Wellman for their technical support.

# ABSTRACT

An intermittency model that is formulated in local variables is proposed for representing bypass transition in Reynolds-Averaged Navier-Stokes (RANS) computations. No external data correlation is used to fix transition. Transition is initiated by diffusion and a source term carries it to completion. A sink term is created to predict the laminar region before transition and vanishes in turbulent region. The present model is implemented in OpenFOAM, a platform for computational fluid dynamics (CFD) codes with unstructured mesh. For validation of this model, a group of test cases based on flat plate experiments have been set up for numerical simulations in OpenFOAM. It turns out that the current model is capable to predict boundary layer transition on a flat plate both with and without pressure gradients when decent agreement with the available experiment data is observed.

## Nomenclature

| | |
|---|---|
| $U_i$ | Components of mean velocity |
| $U$ | Magnitude of mean velocity |
| $U_{fs}$ | Local free stream velocity |
| $u_i$ | Components of fluctuation velocity |
| $S_{ij}$ | Mean stain rate tensor, $\frac{1}{2}(\partial_j U_i + \partial_i U_j)$ |
| $\Omega_{ij}$ | Mean rotation rate tensor, $\frac{1}{2}(\partial_j U_i - \partial_i U_j)$ |
| $\rho$ | Density |
| $\mu$ | Kinetic viscosity or molecular viscosity |
| $\nu$ | Kinematic viscosity, $\mu/\rho$ |
| $k$ | Turbulence kinetic energy, $\frac{1}{2}u_i u_i$ |
| $\epsilon$ | Dissipation rate of energy per unit mass |
| $\omega$ | Specific dissipation rate, $\epsilon/C_\mu k$, where $C_\mu \equiv 0.09$ |
| $\nu_T$ | Eddy viscosity |
| $\gamma$ | Intermittency function |
| $R_t$ | Turbulent Reynolds number |
| $R_\nu$ | Vorticity Reynolds number |
| $Re_x$ | Reynolds number based on x-coordinate |
| $C_f$ | Skin friction coefficient |
| $y$ | Distance to the nearest wall |
| $y^+$ | Non-dimensional distance in the wall coordinate, $\frac{u^* y}{\nu} = \sqrt{\frac{\tau_w}{\rho}}\frac{y}{\nu}$ |
| $\tau_w$ | Wall shear stress |

*Subscript*

| | |
|---|---|
| $i$ | i=1,2,3 represent the three directions in Cartesian coordinates |

# CHAPTER 1. OVERVIEW

An intermittency model that is formulated in local variables is developed for predicting bypass transition in RANS simulations. No external data correlation is used to fix transition. Transition is initiated by diffusion and a source term carries it to completion. Note that the intermittency function is generally initialized to be unity within the whole domain, which is already a solution to a diffusion equation. To void this trivial solution, a sink term is created to force the intermittency to be zero in the laminar boundary layer before transition and vanishes in turbulent region. The present model is implemented in OpenFOAM, a platform for CFD codes with unstructured mesh, by modifying the existed module for $k-\omega$ RANS turbulent model. For validation of this model, a group of test cases based on flat plate experiments have been set up for numerical simulations in OpenFOAM. It turns out that the current model is capable to predict boundary layer transition on a flat plate both with and without pressure gradients when decent agreement with the available experiment data is observed. Separation induced transition will be taken into consideration in appendix section, and more separation related cases remain to be tested to improve the performance of the model.

This chapter will cover the background knowledge and motivation of the present work, and a brief introduction on the categories of laminar-to-turbulent transition and the research in the past of transition modeling through a literature view.

## 1.1 Introduction

While plenty of models for a wide range of fully turbulent flows are available in general CFD codes, effective models for laminar-to-turbulent transition have not been developed and applied extensively.

One of the difficulties to develop a transition model is that transition takes place through different mechanisms in term of various engineering flows. In aerodynamics, when free-stream turbulence intensity (FSTI) is less than 0.5% ($u^{'}/U < 0.005$), transition typically occurs with intervention of viscous Tollmien-Schilichting instability waves. These waves grow linearly first and eventually lead to a non-linear break-down to turbulence. This kind of transition is generally referred to as natural transition. Another transition mechanism is called bypass transition, which happens when FSTI is about 0.5% or greater without the occurrence of linear instability. Turbulent diffuses into the laminar boundary layer, generates disturbances knows as Klebanoff modes. Figure(1.1) is a plane view of the jets, observed in contours of the $u$ (top) and $v$ (bottom) component of perturbation velocity. These streaky features, seen at the left-hand side of the $u$ contours, are often called Klebanoff modes. The disturbances grow in amplitude and the flow transits to turbulence. In addition, separated-induced transition is another important mechanism, in which a laminar boundary layer separates under the influence of a pressure gradient and transition occurs within the separated shear layer. It is difficult to develop a model which is valid for all different mechanisms mentioned above.

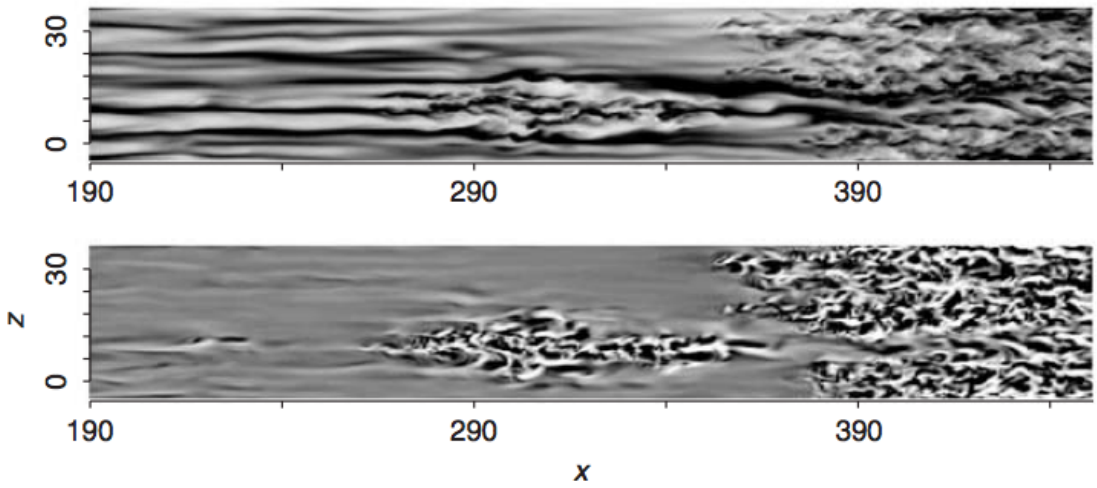


Figure 1.1 Contours of $u$ (top) and $v$ (bottom) in a plane near the wall under conditions of bypass transition (Durbin (2011)).

The present work is to develop a model that invokes an intermittency function to represent bypass transition based on RANS $k-\omega$ turbulent model. In addition to the two transport

equations of kinetic energy ($k$) and specific turbulence dissipation rate ($\omega$), respectively, another transport equation of intermittency ($\gamma$) is combined into the new model.

The fraction of time that the flow at any point is turbulent is called the intermittency. The value of $\gamma$ varies from unity within free-stream turbulent flow to zero in the laminar boundary layer. The function $\gamma$ is used to suppress production of turbulent kinetic energy. Bypass transition is initiated through the diffusion of free-stream disturbances into the laminar boundary layer.As $\gamma$ rises from zero toward unity within the boundary layer, production switches on and the eddy viscosity rises. Meanwhile, in order to have the laminar boundary layer before transition, a certain form of sink term in $\gamma$ equation may be invoked to work within the boundary layer to drive $\gamma$ towards zero.

## 1.2 Literature Review

### 1.2.1 Transition Modes

In this section, a brief review is given on previous research of various modes by which transition is believed to occur.

#### 1.2.1.1 Natural transition

In early research on inviscid stability theory, a famous and useful general result is that the occurrence of an inflection point in the basic velocity profile is a necessary condition for instability. Later on, solutions to viscous instability problem (Orr-Sommerfeld problem) were first found numerically by Tollmien and Schlichting. When the free-stream turbulence level is low ($< 0.5\%$), a laminar boundary layer becomes linearly unstable at sufficient Reynolds number: the instability takes the form of two-dimensional waves, the so called Tollmien-Schlichting waves. Since the growth rate is so slow, transition to turbulence might not complete until a stream-wise distance is as large as 20 times farther downstream from the leading edge than the initial starting point of linear instability. The transition occurs only after the waves become nonlinear and three-dimensional disturbances take over. At this position turbulent spots start to appear, which grow in the surrounding laminar layer and then grow and merge to form the

fully turbulent boundary layer. This type of transition is referred to as natural transition.

#### 1.2.1.2 Bypass transition

Under free-stream turbulence level of about 0.5% or more, boundary layers proceed from laminar to fully turbulent without the occurrence of linear instability of the base state so that turbulent spots are directly produced within the boundary layer. In other words, this kind of transition occurs bypassing the linear instability stage such that it is called bypass transition. It is often argued that for bypass transition, linear stability is irrelevant and to date no one has been able to detect Tollmien-Schlichting waves when the free-stream turbulence level was greater than 1.0%. It should be noted that bypass transition can also happen due to surface roughness where the disturbances are activated from the perturbations at the wall instead of from the free-stream turbulence.

#### 1.2.1.3 Separated flow transition

When a laminar boundary layer separates, transition may occur in the shear layer of the separated flow as a result of the inviscid instability mechanism. Due to the enhanced mixing caused by the turbulent flow, the shear layer may reattach. This reattachment forms a laminar-separation/turbulent-reattachment bubble on the surface. This type of transition can occur as a result of separation due to a strong adverse pressure gradient.

### 1.2.2 Transition Models

Three approaches have been devised: rely on the closure model to transition from laminar to turbulent solutions; use a data correlation to decide when to switch from laminar to turbulent solutions; or devise additional model equations to represent transition. In the last approach, two branches have been explored:

▲ the first is to develop an equation for the intermittency function, $\gamma(\boldsymbol{x},t)$;

▲ the second is to develop an equation for the energy of fluctuations that occur in the laminar region upstream of transition.

#### 1.2.2.1 Reliance on the turbulent model

Most turbulent models are developed for fully turbulent flows and calibrated with turbulent data. However, most transport equation models do converge to a laminar solution at low Reynolds number and to a turbulent solution at sufficiently high Reynolds number. The model equations do evidence a transition between laminar and turbulent solution branches. Most eddy viscosity closure models predict early transition.

It is common to encounter regions of purely laminar, or buffeted laminar, flow in applications. For instance, turbine blades often operate at low enough Reynolds numbers to come across significant portions of laminar flow on their surface-the blades are subjected to external turbulence, so their boundary layers are better described as buffeted laminar layers. In such instances, the bulk of the flow may be turbulent and the overall flow calculation must be with a turbulence model. Bypass transition which comes into play in this case is stochastic by nature. Turbulent spots are highly localized, irregular motions inside the boundary layer. So the turbulent models which describe statistical fluid dynamics are not entirely irrelevant; but neither are they entirely rational. Very often the models are solved without revision, depending on their capability of early transition prediction. But when accurate predictions of the laminar and transitional regions are required, the turbulence model must be modified by a method to predict transition.

One approach is to switch from a laminar to a turbulent computation at a prescribed transition point. For boundary layers under free-stream turbulence, the data correlation

$$R_{\theta tr} = 163 + e^{6.91 - Tu} \tag{1.1}$$

was proposed by Abu-Gannam and Shaw (1980) for zero pressure-gradient boundary layers. Tu is the turbulence intensity in percentage, $100\sqrt{\bar{u}^2}/U$, measured in the free stream. Transition occurs where the local momentum thickness Reynolds number exceeds the above critical value.

Another approach is to modulate either the eddy viscosity or the production term in the $k$ equation to increase it from zero to its full value across a transition zone. The basic idea is to introduce an intermittency function, $\gamma$, that increases from zero to unity, and to replace the

eddy viscosity by $\gamma\nu_T$. If the transition has been predicted to occur at $x_{tr}$ by making use of the transition criterion in equation (1.1), formulas like

$$\gamma = 1 - e^{-(x-x_{tr})^2/l_{tr}^2}, \qquad x \geqslant x_{tr}, \tag{1.2}$$

have been used. $\gamma$ is slowly ramped up from zero to unity until the fully turbulent boundary is achieved. Here $l_{tr}$ is a transition length, which has been estimated to be about 126 times the momentum thickness ($l_{tr}$=126 $\theta$) in zero pressure-gradient boundary layers.

#### 1.2.2.2 Intermittency transport equation

A relatively new approach to intermittency modeling is to propose a transport equation for the intermittency factor where the source terms are devised to mimic the behavior of some algebraic intermittency models, such as equation (1.2). This equation can be derived into a transport equation. Note that for $x > x_{tr}$.

$$\frac{d\gamma}{dx} = 2\frac{x - x_{xr}}{l_{tr}^2} e^{-(x-x_{tr})^2/l_{tr}^2} = 2\frac{1-\gamma}{l_{tr}} \left[-log(1-\gamma)\right]^{1/2}.$$

If x is regarded as the stream-wise direction, this can be generalized to

$$\mathbf{u} \cdot \nabla\gamma = |\mathbf{u}| \frac{2(1-\gamma)}{l_{tr}} \left[-log(1-\gamma)\right]^{1/2}.$$

If $\gamma$ is small $\sqrt{-log(1-\gamma)} \approx \sqrt{\gamma}$. Adding a diffusion term provides a transport equation

$$D_t\gamma = 2(1-\gamma)\sqrt{\gamma}\frac{|\mathbf{u}|}{l_{tr}} + \nabla \cdot [(\nu + \nu_T)\nabla\gamma]. \tag{1.3}$$

This is a starting point for more elaborate formulations. The main advantages of this approach is that it is possible to model the transition process not only in the flow direction but also across the boundary layer and thus provide a more realistic prediction of the transition. The transport equation controls the rise of $\gamma$ from zero in laminar flow to unity in turbulent flow. The onset position of transition still has to be determined by a data correlation like equation(1.1). The correlation involves the boundary layer momentum thickness and the free-stream turbulence. The former is an integral property and the latter a remote variable. This is unsuitable for

unstructured-grid CFD codes. Otherwise in boundary layer codes or structured-grid CFD codes, this approach is feasible since the grid lines are aligned normal to the wall and the required variables can be obtained by searching in the grid j coordinate (i.e. in the wall normal direction by assuming the grid is strictly aligned with the wall).

To implement such equation in unstructured-grid CFD codes for more general engineering circumstances, some models which are formulated in only local variables are developed (Langtry and Menter (2009)). In their method, the data correlation is replaced by a transport equation for transition Reynolds number (1.4). The intermittency function solves a second transport equation (1.5).

$$D_t Re_{\theta t} = P_{\theta t} + \nabla \cdot [2.0(\nu + \nu_T)\nabla Re_{\theta t}], \tag{1.4}$$

$$D_t \gamma = P_\gamma - E_\gamma + \nabla \cdot [(\nu + \nu_T)\nabla \gamma]. \tag{1.5}$$

The source term $P_\gamma$ and sink term $E_\gamma$ are defined as follows,

$$P_\gamma = 2.0|S|(1-\gamma)(\gamma F_{onset})^{0.5} F_{length}, \tag{1.6}$$

$$E_\gamma = 0.06|\Omega|\gamma(50\gamma - 1)F_{turb}, \tag{1.7}$$

where $|S|$ is the magnitude of mean strain rate tensor, and $|\Omega|$ is the magnitude of the mean rotation rate tensor. $F_{length}$ is an empirical correlation that controls the length of transition, and $F_{onset}$ controls the transition onset location. The form of $F_{onset}$ is as follows,

$$\begin{aligned} F_{onset1} &= \frac{Re_\nu}{2.193 \cdot Re_{\theta c}} \\ F_{onset2} &= \min(\max(F_{onset1}, F_{onset1}^4), 2.0) \\ F_{onset3} &= \max\left(1 - \left(\frac{R_t}{2.5}\right)^3, 0\right) \\ F_{onset} &= \max(F_{onset2} - F_{onset3}, 0), \end{aligned} \tag{1.8}$$

where

$$R_t \equiv \frac{\nu_T}{\nu}$$
$$R_\nu \equiv \frac{d^2|\Omega|}{2.193\nu}. \tag{1.9}$$

Note that the criterion of onset is now controlled by a local parameter $R_\nu$ instead of a integral parameter $R_{\theta t}$ in equation (1.1). So far, $Re_{\theta c}$ and $F_{length}$ still need to be determined so as to let production term (1.6) be well defined. In Langtry and Menter (2009), these two variables are both functions of $Re_{\theta t}$, which is the solution of equation (1.4). Data correlations are used to construct the functions for $Re_{\theta c}$ and $F_{length}$.

The idea is similar to earlier models that specify transition location, then solve a $\gamma$-equation to represent the transitional zone. But in Langtry and Menter (2009) the data correlation involved in the source term $P_{\theta t}$ in equation (1.4) invokes the mean velocity and the streamline direction. That data correlation is not Gallilean invariant, which is problematic for multiple moving walls in the domain.

Another key point is the sink term $E_\gamma$ in equation (1.5). The effect of this is to drive $\gamma$ towards zero in laminar boundary layer so that a trivial solution $\gamma = 1$ can be avoided. This idea is also used in the present model. More discussion will be given below.

For the purpose of explanation, the model introduced above is not exactly the same as the one in Langtry and Menter (2009). More parameters and complicated correlations are used to match the experimental data.

#### 1.2.2.3 Laminar fluctuation model

As mentioned above, another approach is devised with a transport equation for the energy of fluctuations in the laminar boundary layer-the Klebanoff modes or instability waves-and has closer connection to the phenomenology of transition.

These fluctuations grow and produce turbulent kinetic energy. The key elements of the equation for laminar fluctuations are production and transfer to turbulence. Walters and Cokaljat (2008) propose the form

$$D_t k_L = 2\nu_{Tl}|S|^2 - R - D_L + \nabla \cdot \ (\nu \nabla k_L), \tag{1.10}$$

in which $2\nu_{Tl}|S|^2$ is the rate of production of laminar fluctuations, $D_L$ is a destruction term, and R will be described below. To accommodate both bypass and natural transition, $\nu_{Tl}$ has two components,

$$\nu_{Tl} = \nu_{BP} + \nu_{NT},$$

associated with large-scale eddies and with instability.

Initially, the large-scale eddies are contained in free-stream turbulence. Klebanoff modes are spawned by these large-length-scale motions. The model is motivated by this phenomenology. Walters and Cokaljat (2008) write

$$v_{BP} = 3.4 \times 10^{-6} f_{\tau l} \frac{\Omega \lambda_{eff}^2}{\nu} \sqrt{k_{Tl}} \lambda_{eff}, \tag{1.11}$$

with

$$\lambda_{eff} = min[2.495d, \sqrt{k}/\omega]$$

providing the length scale; and

$$k_{Tl} = k \left[ 1 - \left( \frac{\lambda_{eff}}{L} \right)^{2/3} \right],$$

where $L = \sqrt{k}/\omega$, representing the large-scale component of the turbulent kinetic energy. The laminar fluctuation equation(1.10) is conjoined with the k-$\omega$ model.

In equation(1.11), $\Omega$ is the magnitude of the vorticity vector; and $f_{\tau l}$ is the damping function

$$f_{\tau l} = 1 - exp \left[ -4360 \frac{k_{Tl}}{2\lambda_{eff}^2 |S|^2} \right].$$

The numerical coefficients were adjusted to fit data. They control the onset of transition just like functions like $f_{onset}$ in intermittency models. The component $\nu_{BP}$ becomes small where $d$ is large and where $d$ is small. This matches the exponential observation that Klebanoff modes develop in the central part of the boundary layer.

Natural transition is invoked by

$$\nu_{NT} = 10^{-10}\beta_L \frac{\Omega d^2}{\nu}\Omega d^2, \tag{1.12}$$

with

$$\beta_L = \begin{cases} 0, & R_\Omega > 1000, \\ 1 - e^{-(0.005R_\Omega - 5)}, & R_\Omega > 1000, \end{cases}$$

where $R_\Omega = \Omega d^2/\nu$. This acts analogously to an instability criterion. In a Blasius boundary layer, $\max_y R_\Omega = 2.193R_\theta$. Thus the instability criterion is $R_\theta > 456$ (which is higher than the value of 200 from linear stability theory).

The term R in equation(1.10) represents breakdown of laminar fluctuations into turbulence. The same term, with positive sign, is added to the turbulent kinetic energy equation: $D_t k = P + R - \epsilon \ldots$. Its form is

$$R = 0.21B_L \frac{k_L}{\tau_T},$$

where $\tau_T = \lambda_{eff}/\sqrt{k}$. As the turbulent energy grows, $\tau$ decreases, transferring energy from laminar fluctuations to turbulence. The coefficient $B_L$ controls the onset of transition,

$$B_L = \begin{cases} 0, & R_k > 35, \\ 1 - e^{-(R_k - 35)/8}, & R_k > 35, \end{cases}$$

where $R_k = \sqrt{k}d/\nu$. The transition criterion is based on the Reynolds number $R_k$, which contains wall distance and turbulent kinetic energy. Thus breakdown initiates well above the wall, as occurs in experiments.

Walters and Cokaljat (2008) also modify R for natural transition, and introduce other limiting and interpolation functions to improve agreement with data.

# CHAPTER 2. DEVELOPMENT OF THE MODEL

## 2.1 Introduction

In this chapter, the development of the present model will be described. The rationals of different terms in the model as well as the parameter sensitivity will be given by conducting simulations on some simple test cases.

## 2.2 The Form of The Model

This specific model is based on the standard $k-\omega$ RANS closure (Wilcox (1993)). It is a two-equation turbulence model (see equation (2.1) and (2.2)). One is a transport equation for turbulent kinetic energy, and the other is for specific dissipation rate.

$$\frac{Dk}{Dt} = 2\nu_T|S|^2 - C_\mu k\omega + \partial_j\Big[\Big(\nu + \frac{\nu_T}{\sigma_k}\Big)\partial_j k\Big] \tag{2.1}$$

$$\frac{D\omega}{Dt} = 2C_{\omega 1}|S|^2 - C_{\omega 2}\omega^2 + \partial_j\Big[\Big(\nu + \frac{\nu_T}{\sigma_\omega}\Big)\partial_j \omega\Big] \tag{2.2}$$

where $C_\mu = 0.09, C_{\omega 1} = 5/9, C_{\omega 2} = 3/40$ and $\sigma_\omega = \sigma_k = 2$.

The intermittency function ($\gamma$) is placed into the production term ($2\nu_T|S|^2$) of the $k$-equation. This is the only appearance of $\gamma$ in the turbulence model, hence equation (2.1) becomes

$$\frac{Dk}{Dt} = 2\gamma\nu_T|S|^2 - C_\mu k\omega + \partial_j\Big[\Big(\nu + \frac{\nu_T}{\sigma_k}\Big)\partial_j k\Big], \tag{2.3}$$

and there is no change in equation (2.2). Here $|S|^2 = S_{ij}S_{ji}$ is the square of magnitude of the mean rate of strain tensor. The eddy viscosity is defined as

$$\nu_T = k/\omega. \tag{2.4}$$

Theory and computer simulations of bypass transition indeed attribute its initiations to diffusion of free-stream turbulence into the boundary layer. They also show that only low frequencies can penetrate the boundary layer (Zaki and Durbin (2005)). Similarly, Praisner and Clark (2007) suggest that turbulent time-scale plays a major role in transition, and its interesting implication is that when turbulence scale is included, pressure gradients and other parameters are secondary. All these above give the rational of the current simple model with only one transport equation of intermittency.

In the present context, intermittency does not have a definite physical meaning. The function $\gamma$ is used to suppress production of turbulent kinetic energy. In laminar flow $k = 0$ and $\nu_T = 0$. When $\gamma$ is small, equation (2.3) will force $k$ to be small. $\gamma$ is supposed to be zero inside the laminar boundary layer and unity in free-stream turbulent region. Non-zero $\gamma$ will diffuse into the boundary layer, enhancing the production of $k$, increasing eddy viscosity, and hence initiating the transition. On other words, transition is controlled by penetration of free-stream turbulence into the boundary layer via molecular and turbulent diffusion.

Consider an intermittency transport equation of the form

$$\frac{D\gamma}{Dt} = \partial_j\left[\left(\frac{\nu}{\sigma_l} + \frac{\nu_T}{\sigma_\gamma}\right)\partial_j\gamma\right] + F_\gamma|\Omega|\left(\gamma_{max} - \gamma\right)\sqrt{\gamma} - C_1 G_\gamma F_{turb}|\Omega|\gamma^{1.5} \tag{2.5}$$

with initial conditions $\gamma = 1$ in the whole domain and $\partial_n\gamma = 0$ on walls. $\Omega$ is the magnitude of the mean rotation rate tensor.

Excluding the sink term, i.e. the third term in the right-hand side, equation (2.5) would have identical form as the $\gamma$-equation in Durbin (2012). The diffusion term initiates the transition and the source term completes it.

### 2.2.1 Diffusion Term

The influence of the two constants $\sigma_l$ and $\sigma_\gamma$ in the diffusion term on the transition is given below. They are set to be 5.0 and 0.2,respectively.

From the diffusion term itself, we can predict that increasing $\sigma_\gamma$ decreases turbulent diffusivity and delays transition, and vice versa. In the current model, $\sigma_\gamma$ is selected to be 0.2. If it is doubled or even greater, the diffusion is suppressed and the transition delayed. An issue that

has to be pointed out is that this parameter become less sensitive once it is less than 0.2. When it is halved, the result changes very slightly; but it does give obvious early transition if $\sigma_\gamma$ is 0.02 or even smaller. It is due to the sink term which is designed to drive $\gamma$ to zero in order to have laminar region before transition. After transition, the sink is supposed to vanish and hence just doubling the proper value of $\sigma_\gamma$ affects the result significantly. See figure (2.1). The plots in this figure are the skin friction coefficient, $C_f$ curve through the stream-wise direction of a flat plate test case, T3A, one of the T3 series of flat-plate experiments conducted by the European Research Community on Flow Turbulence and Combustion (ERCOFTAC).

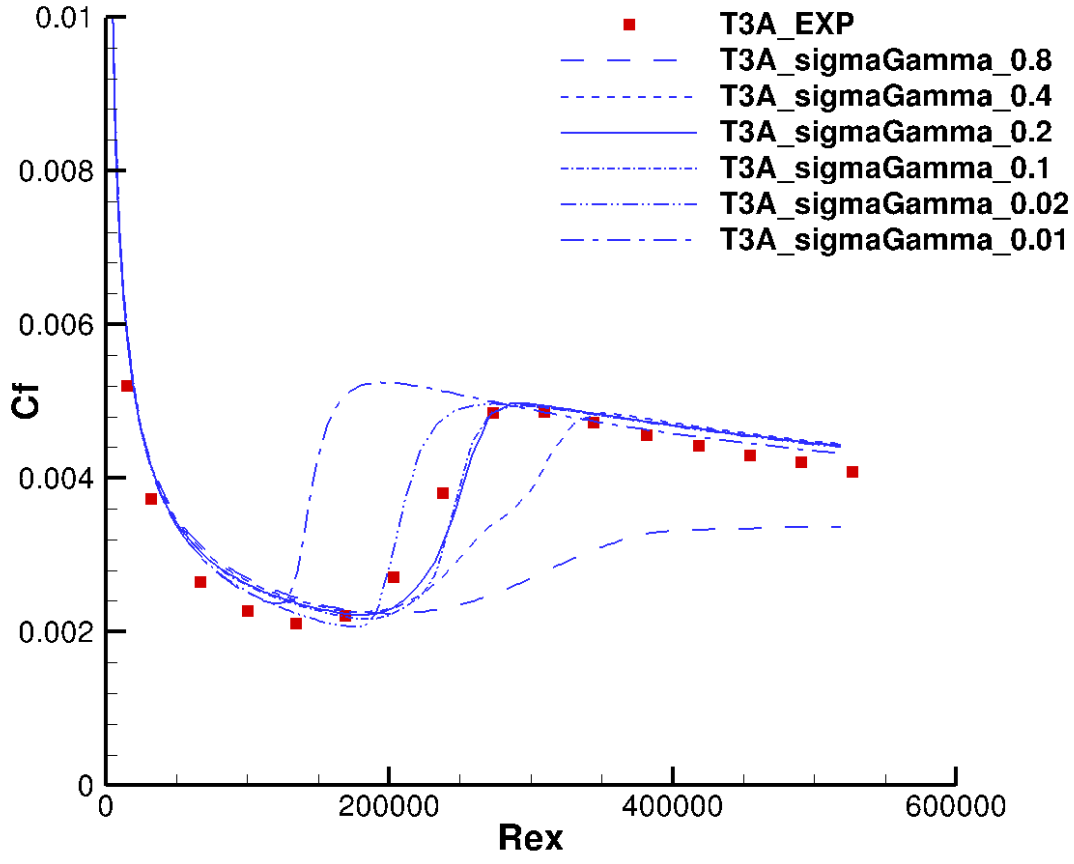


Figure 2.1 Sensitivity of $\sigma_\gamma$ to the transition location. The proper value of $\sigma_\gamma$ is 0.2. When it is doubled, transition delay can be recognized; but when it is halved, the effect is very little.

However, the effect of $\sigma_l$ is a little bit unintelligible. When it is doubled, the $C_f$ curve goes up from the proper results with early transition, whereas transition occurs further downstream if $\sigma_l$ is halved. It turns out to be a reverse effect of $\sigma_\gamma$. See figure (2.2).

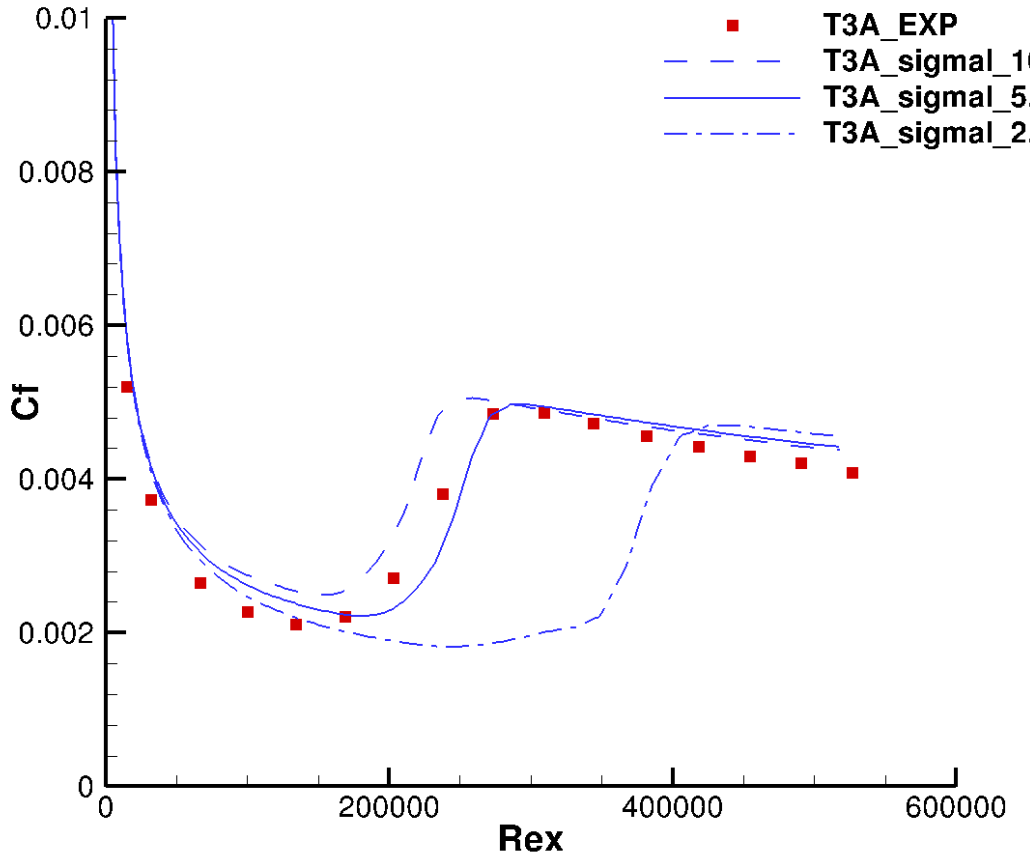


Figure 2.2 Sensitivity of $\sigma_l$ to the transition location.

### 2.2.2 Source Term

Note that $\gamma_{max}$ instead of unity is placed in the source term compared with $P_\gamma$ in equation (1.6). This is in order to enhance the effect of the source term to drive $\gamma$ to one. Accordingly, $\gamma$ is possible to exceed unity due to such source, which is not allowed. After each step of the computation, $\gamma$ is forced to the value of $\min(\gamma, 1)$ to chop off values greater than unity. This has a small effect, but it does force a full transition to turbulence if $\gamma$ is guaranteed to be unity

after transition.

The factor $F_\gamma$ switches on as transition proceeds. Once it comes into play, $\gamma$ will increase up to unity within the region $F_\gamma$ affects. Therefore, turbulent kinetic energy $k$ increases as well as the eddy viscosity. Meanwhile, the sink term vanishes and the transition model turns into fully turbulent model.

$F_\gamma$ is a function of two parameters. In them, mean shear is represented by the magnitude of the mean rotation rate $|\Omega|$ (i.e. $\sqrt{2 \cdot \Omega_{ij}\Omega_{ji}}$). It recalls that turbulence is caused by mean shear. $|\Omega|$ is an invariant measure of shear, and it vanishes in the irrotational free-stream.

Three non-dimensional parameters are involved,

$$\begin{cases} R_t \equiv \dfrac{\nu_T}{\nu} \\ R_\nu \equiv \dfrac{d^2|\Omega|}{2.188\nu} \\ T_\omega \equiv R_t \dfrac{|\Omega|}{\omega} \end{cases} \tag{2.6}$$

where $d$ is distance to the wall. $R_t$ is the ratio of eddy viscosity to molecular viscosity, namely the turbulent Reynolds number. $R_\nu$ is the vorticity Reynolds number, which depends only on local variables. Note that near a wall in the constant stress layer it goes like wall distance square, i.e. $R_\nu \to y_+^2/2.188$, as $y_+ \to 0$. It is defined as such that the maximum of the profile in normal wall direction is equal to the momentum thickness Reynolds number: $\max_y R_\nu = R_\theta$. When the boundary layer is applied by pressure gradients, the relationship between momentum thickness and vorticity Reynolds number will change due to the change of the profile of $R_\nu$. In Falkner-Skan boundary layers $\max_y R_\nu$ is less than $R_\theta$ for favorable pressure gradients and greater than $R_\theta$ for adverse pressure gradients. So a fixed value of $R_\nu$ will correspond to a higher $R_\theta$ for favorable pressure gradients and a lower $R_\theta$ as the pressure gradient becomes adverse.

The parameter $T_\omega$ is $R_t$ multiplied by $|\Omega|/\omega$ to make it vanish in the free-stream. Another view of $T_\omega$ is that in parallel flow $T_\omega = |\overline{uv}|/\nu\omega$. In log-layer it equals to $u_*^2/\nu\omega = 1/\omega_+$.

The function $F_\gamma$ is determined by the two parameters $R_\nu$ and $T_\omega$. $T_\omega$ is used to form a critical Reynolds number, $R_c$. It is a decreasing function of $T_\omega$. If the turbulent intensity is low, $T_\omega$ will

be low and $R_c$ will be high. See equation (2.7). $R_c$ has a linear ramp down between 400 and 40.

$$R_c = 400 - 360 \min\left(\frac{T_\omega}{2}, 1\right) \tag{2.7}$$

As the local Reynolds number $R_\nu$ crosses $R_c$ from below, $F_\gamma$ ramps up from zero. Again a linear ramp up is used. Meanwhile, a ramp down is included if the Reynolds number crosses $R_{\nu bound} = 100/0.7$ without the flow becoming turbulent. This approach is to suppress $F_\gamma$, namely the source term to switch on for low free-stream turbulence. The concrete formula for $F_\gamma$ is

$$F_\gamma = 2 \max\left[0, \min\left(100 - 0.7R_\nu, 1\right)\right] \times \min\left[\max\left(R_\nu - R_c, 0\right), 4\right]. \tag{2.8}$$

On other words,

$$F_\gamma = \begin{cases} 0, & if\ R_\nu \leqslant R_c,\ or\ if\ R_\nu \geqslant 100/0.7, \\ 8, & if\ R_\nu > R_c + 4\ and\ R_\nu \leqslant 100/0.7 - 1. \end{cases}$$

Effect of the upper limit 4 in the second factor of the right-hand side of equation (2.8) is

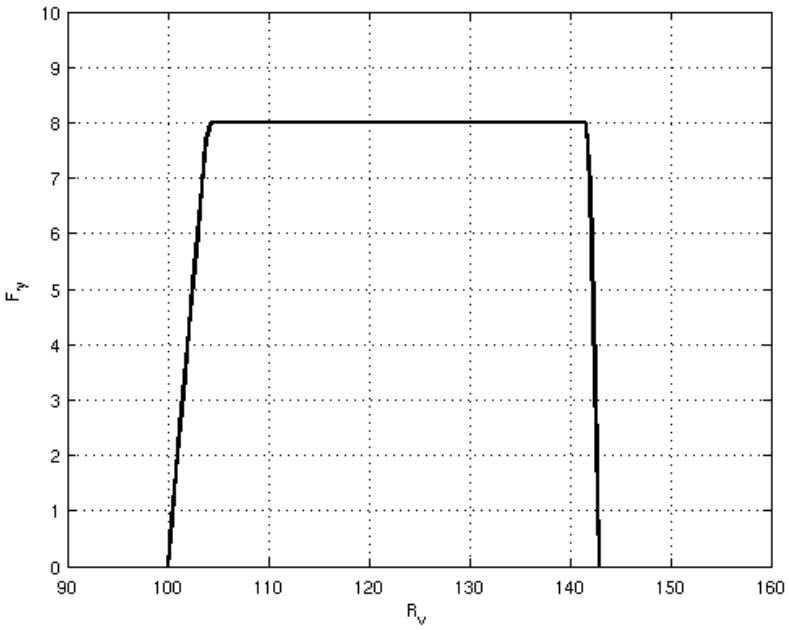


Figure 2.3 $F_\gamma$ vs. $R_\nu$ when $R_c$ is set to be 100.

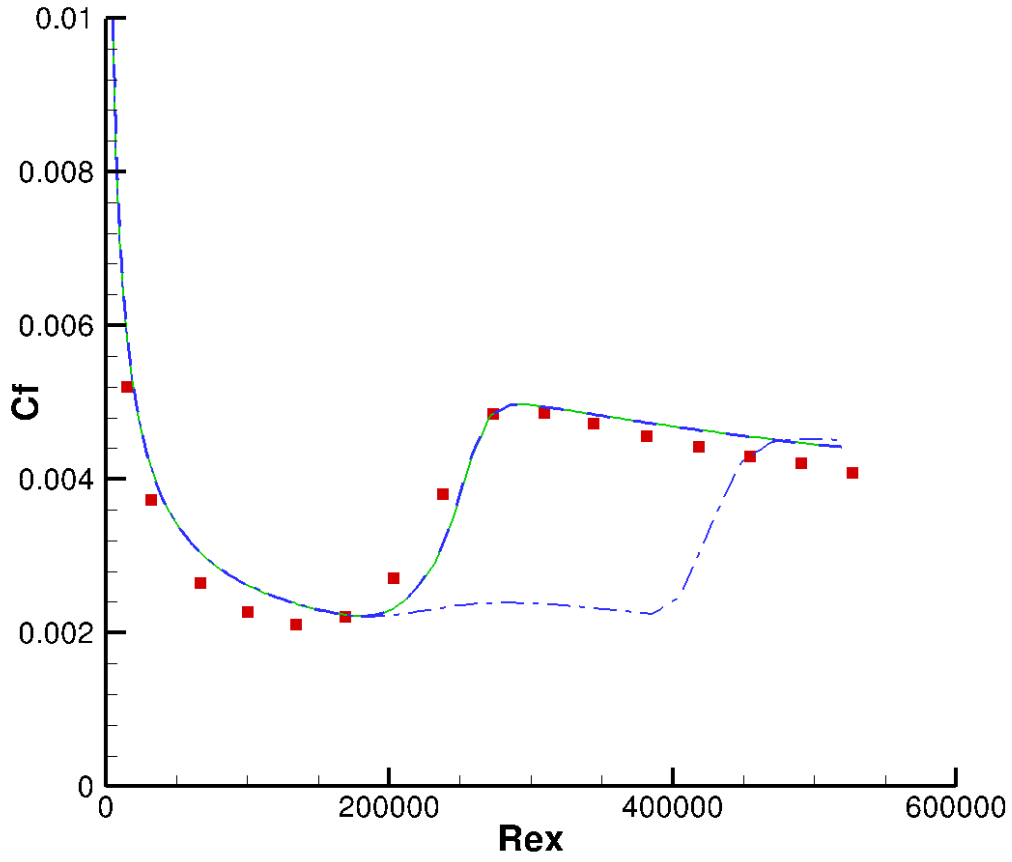


Figure 2.4 $R_{\nu bound}$ is equal to 100/0.5 (blue dash-dot); 100/0.7 (green solid); 100/0.9 (blue dash).

inconsiderable; a greater value does not change the result pretty much. The plot of $F_\gamma$ versus $R_\nu$ is given in figure (2.3), when the critical Reynolds number $R_c$ is 100, which illustrates how $F_\gamma$ ramps up then down. The upper limit of $R_\nu$ where $F_\gamma$ crosses from non-zero to zero ($R_{\nu bound}$) is sensitive to the location of transition. If it is set to be greater than 100/0.7, transition is supposed to be accelerated; if it is less, transition is supposed to be delayed. However, due to the effect of the sink term discussed above in the section on the diffusion term, if for example $R_{\nu bound} = 100/0.5$ is used, the $C_f$ curve will be barely changed rather than showing a obvious early transition. When $R_{\nu bound} = 100/0.9$, it does result in a late transition. See figure (2.4).

### 2.2.3 Sink Term

Without a sink term, the $\gamma$-equation (2.5) would have the solution $\gamma \equiv 1$. The numerical elliptic solver will converge to unity within the whole domain, which will produce fully turbulent results. See figure (2.5).

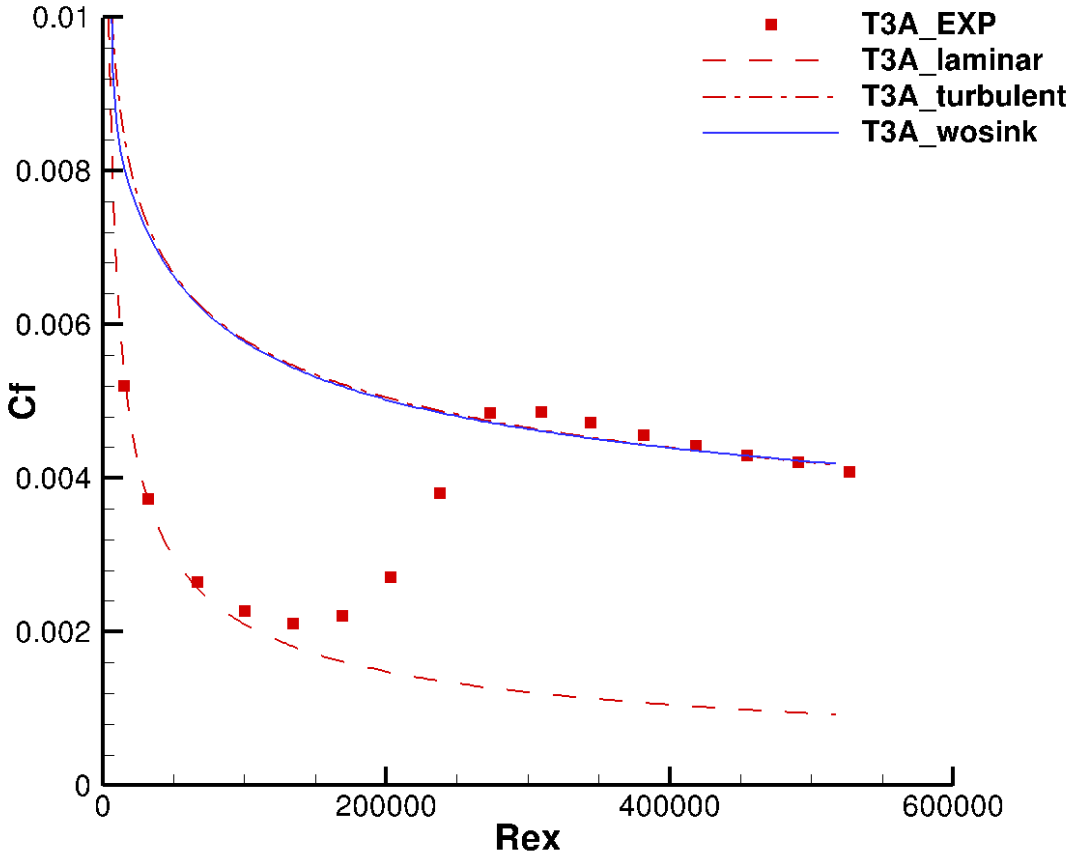


Figure 2.5 Skin friction coefficient vs. $Re_x$ in a flat plate test case (T3A); the blue solid curve represents the result based on the model without sink term. The other three represent the experimental data, theoretical laminar solution, and half-empirical turbulent solution respectively.

In order to force $\gamma$ close to zero within the laminar region, a sink term is added in equation (2.5). Another feature of the sink term is that it has to vanish after transition because $\gamma$ is supposed to be unity in fully turbulent region. This feature is implemented by the multiplication

of two functions, $G_\gamma$ and $F_{turb}$. The definition of $G_\gamma$ is similar to $F_\gamma$ in the source term. See equation (2.9). It is used to ensure the laminar region before transition. It ramps up from $R_\nu = 18$ and ramps down after $R_\nu = 100$.

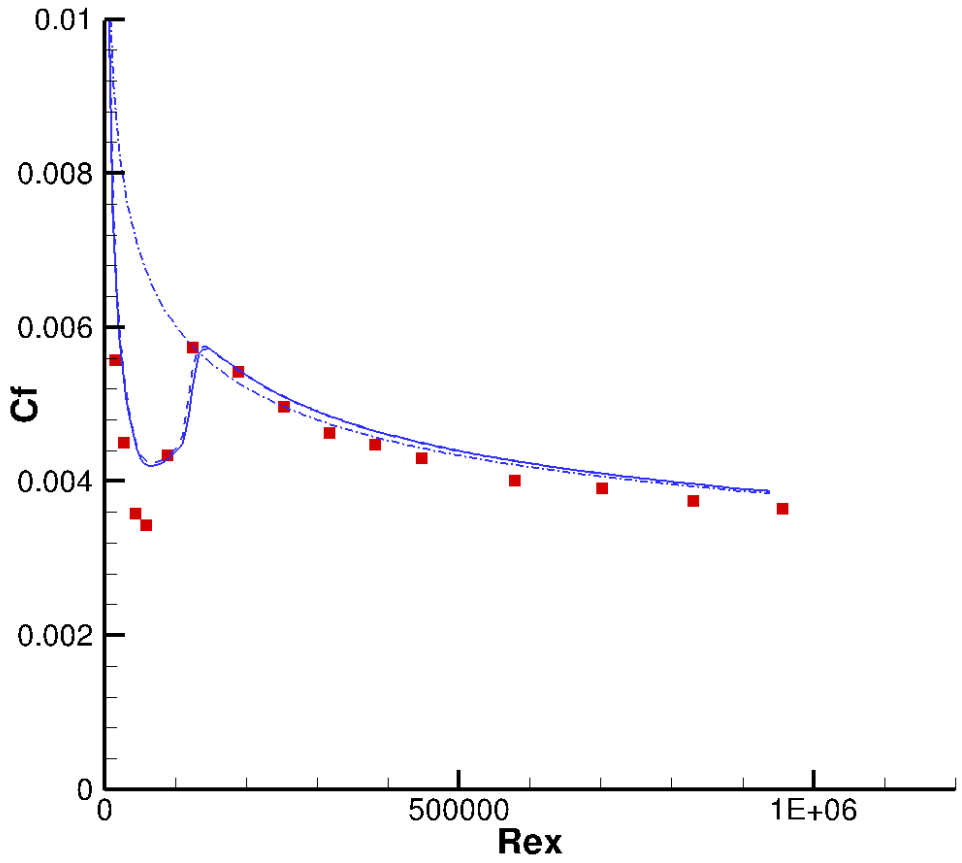


Figure 2.6 $R_{\nu lbound}$ is equal to 18 (blue solid); 20 (blue dash); 22 (blue dash-dot). From 18 to 20, the difference is tiny; but from 20 to 22, $C_f$ curve becomes fully turbulent one.

$$G_\gamma = \max\left[0, \min\left(100 - R_\nu, 1\right)\right] \times \min\left[\max\left(R_\nu - 18, 0\right), 1\right]. \tag{2.9}$$

On other words,

$$G_\gamma = \begin{cases} 0, & if\ R_\nu \leqslant 18,\ or\ if\ R_\nu \geqslant 100 \\ 1, & if\ R_\nu > 19\ and\ R_\nu \leqslant 99. \end{cases}$$

The lower bound $R_{\nu lbound} = 18$ is critical to some extend. Basically, if it equals to 22 or higher, the model will be invalid for high free-stream turbulence intensity cases, like T3B test case. For these cases, the laminar region is relative thin and short. Therefore, a relative high $R_{\nu lbound}$ may not catch the thin laminar region near wall and hence the sink term may vanish. See figure (2.6). Too small value for $R_{\nu lbound}$ is not proper either because the sink term is supposed to vanish after transition. Recall that $R_\nu$ goes like $y_+^2$ near wall and hence too small $R_{\nu lbound}$, say 0, makes $G_\gamma$ non-zero all the way down to the turbulent region with the sink term not vanishing.

$F_{turb}$ is a function of $R_\nu$ and $R_t$. It will vanish outside the laminar boundary layer and the near wall viscous sublayer. It is defined as,

$$F_{turb} = e^{-(R_\nu R_t)^{1.2}}. \tag{2.10}$$

The power 1.2 is selected to match the data. Large value of it will reduce the region where $F_{turb}$ works, which in turn suppresses the sink and leads to early transition. $C_1$ in equation (2.5) is chosen to be 7.5, which represents the strength of the sink term. The larger it is, the later the transition will occur.

# CHAPTER 3. COMPUTATIONS

## 3.1 Introduction

In this chapter, the transition model developed in CHAPTER 2 is used to simulate the T3 series of flat-plate experiments conducted by the European Research Community on Flow Turbulence and Combustion (ERCOFTAC). These experiments were performed at Rolls Royce (Langtry (2006)). The T3 series of test cases (T3A, T3B, T3C1, T3C2, T3C3, T3C4, T3C5) have often been used as a benchmark for transition simulation by bypass transition models. Test cases T3A and T3B have a zero stream-wise pressure gradient with different turbulence intensities. Test cases T3C series combine the influences of free-stream turbulence and favorable/adverse pressure gradients imposed by the converging/expanding flow channel. They are chosen to be representative of an aft-loaded turbine. The main difference between the various T3C test cases is the free-stream velocity, and hence the Reynolds number (T3C1 is an exception, which has high free-stream turbulence intensity and slow energy decay). The greater the Reynolds number is, the earlier the transition occurs. They are designed for testing the ability of transition model to predict transition under the continuous variation of pressure gradient.

All cases are computed in OpenFOAM with the current transition model implemented in it. Since steady incompressible flow is considered, SIMPLE algorithm is employed to solve all transport equations involved in this model. CFD codes in OpenFOAM are based on finite volume discretization. Cell limited Gauss (second order Gaussian integration) linear scheme is chosen for gradient terms; Gauss linearUpwind (first/second order bounded) scheme is chosen for divergent terms; Gauss linear corrected (Unbounded second order conservative) scheme is chosen for Laplacian terms. Gauss-Seidel solver is applied to solve the linear equation system which is obtained by discretization.

### 3.2 Geometry, Mesh and Boundary

Two different domains are used. Both are two dimensional with only one cell in span-wise direction. One is for the zero pressure gradient test cases (T3A and T3B). It is comprised of a flat plate wall with length of 1.5 m and a symmetric flat top surface with height of 0.8 m. The inlet surface is at 0.04 m upstream of the plate leading edge to eliminate an ambiguous specification of free-stream conditions. The narrow bottom surface between the inlet and the plate leading edge is set as symmetric boundary. The inlet boundary has uniformly fixed-value velocity, $U_{in}$, turbulent kinetic energy, $k_{in}$, specific dissipation rate, $\omega_{in}$ and zero pressure gradient. The outlet boundary has zero-gradient $U$, $k$, and $\omega$ along with zero pressure (the reference pressure). See figure (3.1), the mesh is generated by blockMesh in OpenFOAM.

The other is for varying pressure gradient test cases (T3C series), which consists of a flat plate bottom wall with length of 1.65 m and a slip top wall with various height. At the entrance, the gap between the upper and bottom walls is 0.3 m and the gap varies along the stream-wise direction corresponding to the experimental data of the pressure gradient variation. The length of bottom surface between the inlet and the leading edge is 0.15 m and again set as symmetric boundary. Boundary types of inlet and outlet are the same as those of the zero pressure gradient cases. See figure (3.2), the mesh is generated in IcemCFD.

The first neighbor node to the wall is located at $0.01 < y^+ < 0.1$. The mesh in figure (3.1) and figure (3.2) has 170 and 230 grids in stream-wise direction, and 110 grids and 125 grids in wall-normal direction, respectively. More grids in both directions, i.e. finer mesh would not affect the results much. The wall-normal grid space expanding ratio is 1.1, and the stream-wise grid space expanding from the leading edge is 1.05, for both meshes.

To figure out the height of each cross-section along the length of the channel that can reproduce the required pressure gradient variation, local free-stream velocity has been used. Suluksna et al. (2009) have offered an explicit expression for the height of the top surface by using the approach described above with curve fitting.

$$h/D = min[1.231x^6 - 6.705x^5 + 14.061x^4 - 14.113x^3 + 7.109x^2 - 1.900x + 0.950; 1] \quad (3.1)$$

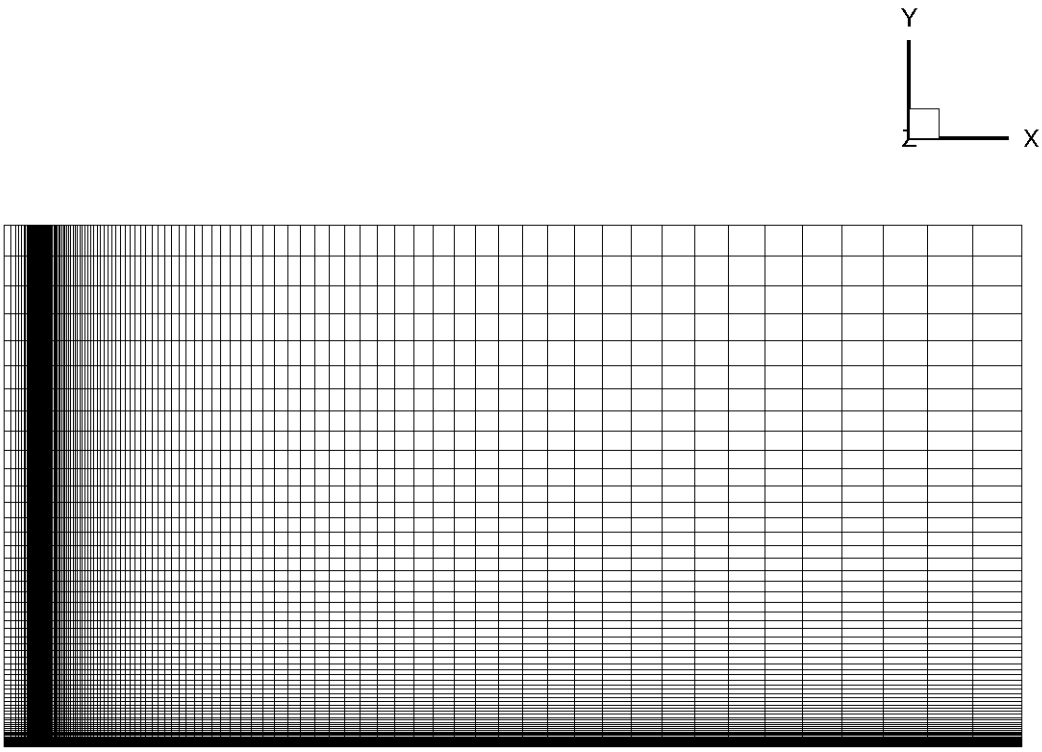


Figure 3.1 Mesh used to compute T3A and T3B cases.

where h is the varying height of the domain and D is the height of the entrance.

## 3.3 Inlet Conditions

The fluid density $\rho$ and the molecular viscosity $\mu$ are 1.2 $kg/m^3$ and $1.8 \times 10^{-5}$ $kg/m \cdot s$, respectively. Then the kinematic viscosity $\nu = \mu/\rho = 1.5 \times 10^{-5}$ $m^2 s^{-1}$. The Reynolds number, $Re_x$, is based on the length from the leading edge and local free-stream velocity. The inlet velocity, $U_{in}$, is specified to match the data of measured local free-stream velocity through the channel. The inlet turbulent kinetic energy $k_{in}$ can be obtained based on the definition of turbulent intensity. See equation (3.2),

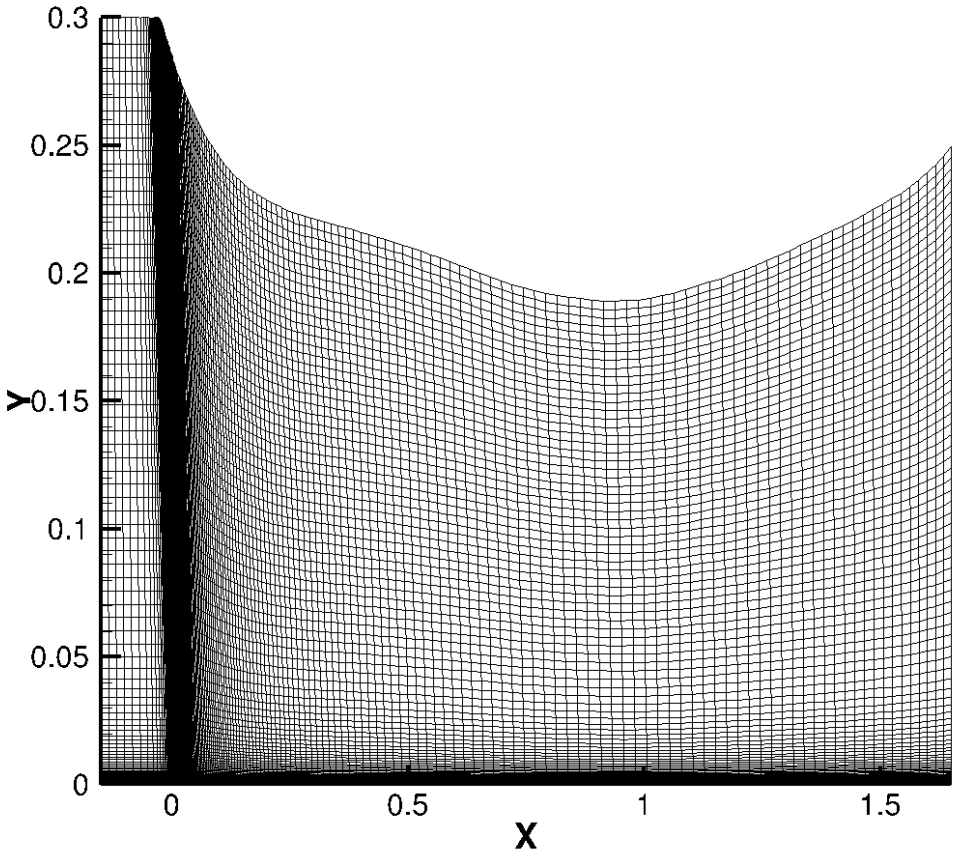


Figure 3.2 Mesh used to compute T3C series cases.

$$Tu_{in} = \frac{\sqrt{2/3k_{in}}}{U_{in}}. \tag{3.2}$$

The inlet viscosity ratio, $R_t$, is used to calculate and specify the inlet specific dissipation rate, $\omega_{in}$,

$$\omega_{in} = \frac{k_{in}}{R_t \nu}. \tag{3.3}$$

Both $Tu_{in}$ and $R_t$ are determined by performing simulation experiments till appropriate agreement with data of the free-stream turbulence intensity decay is obtained. Figure (3.3) and (3.4) show the free-stream velocity and turbulence intensity decay for the T3 series test cases. Good

agreement between simulation results and the experimental data has been obtained by using inlet conditions in table (3.1). There is experimental evidence that both turbulence time-scale and intensity affect bypass transition, i.e. the results are sensitive to the free-stream or inlet conditions. Computations with the current model illustrate this. The results will be shown in the next chapter.

Details of inlet conditions of simulations for different cases are listed in table (3.1).

Table 3.1 Summary of inlet conditions of simulations for different cases

| **Case** | $U_{in}$**(m/s)** | $Tu_{in}$**(%)** | $R_t$ |
|---|---|---|---|
| T3A | 5.2 | 3.5 | 14 |
| T3B | 9.4 | 6.5 | 100 |
| T3C1 | 6.0 | 10.0 | 50 |
| T3C2 | 5.0 | 3.7 | 12 |
| T3C5 | 8.6 | 4.3 | 17 |

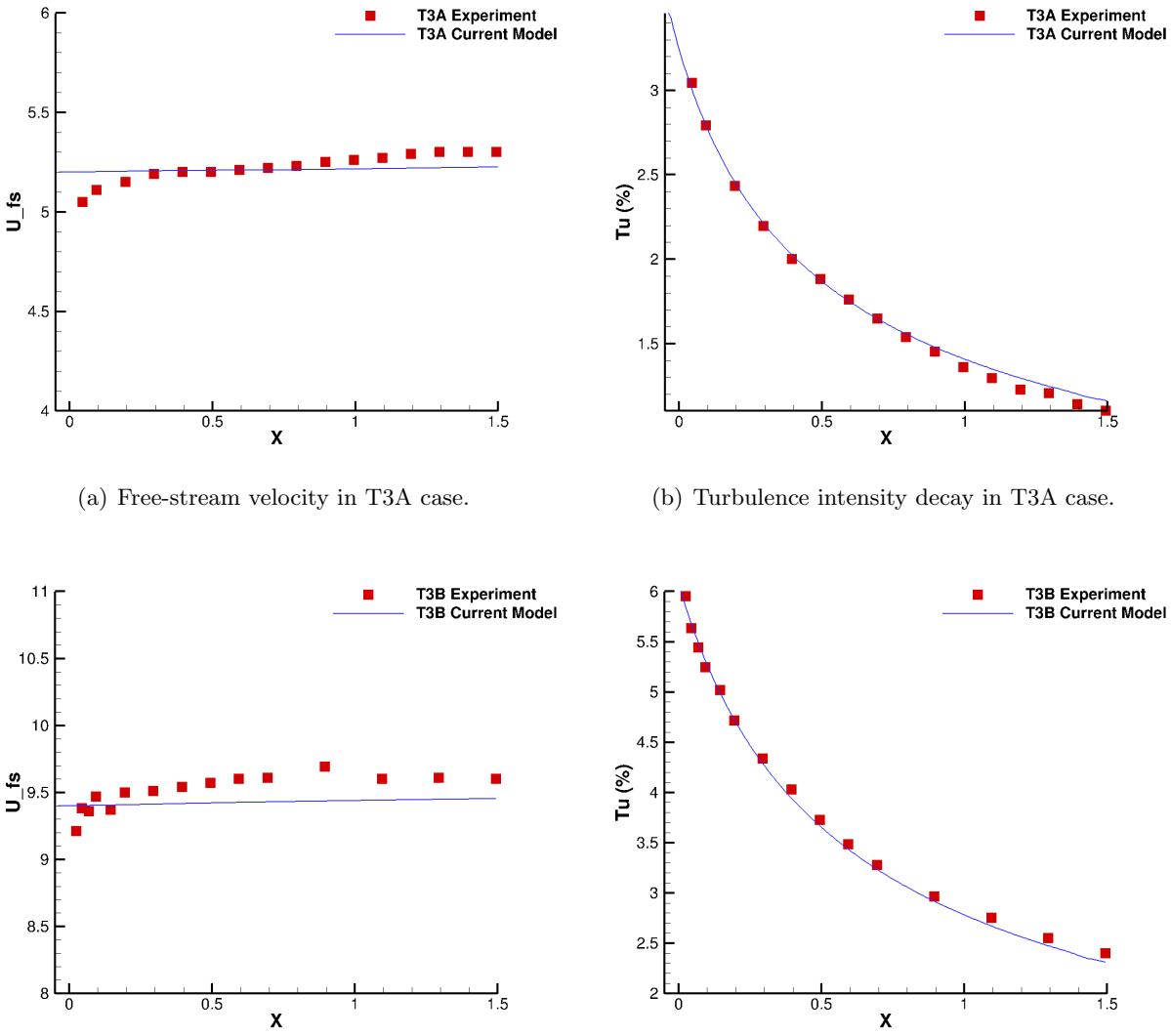


(a) Free-stream velocity in T3A case.

(b) Turbulence intensity decay in T3A case.

(c) Free-stream velocity in T3B case.

(d) Turbulence intensity decay in T3B case.

Figure 3.3 Free-stream velocity and turbulent intensity in T3A and T3B.

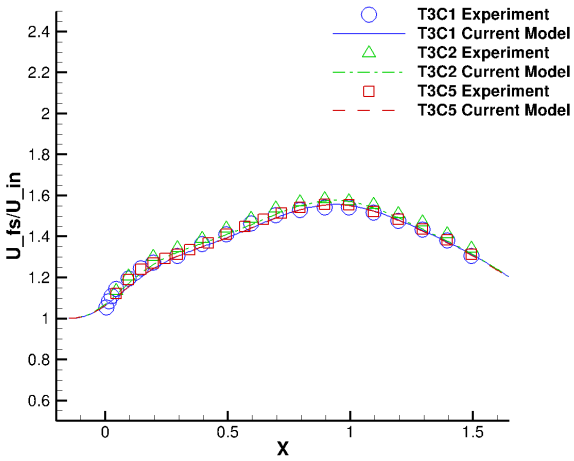


(a) Normalized free-stream velocity in T3C cases.

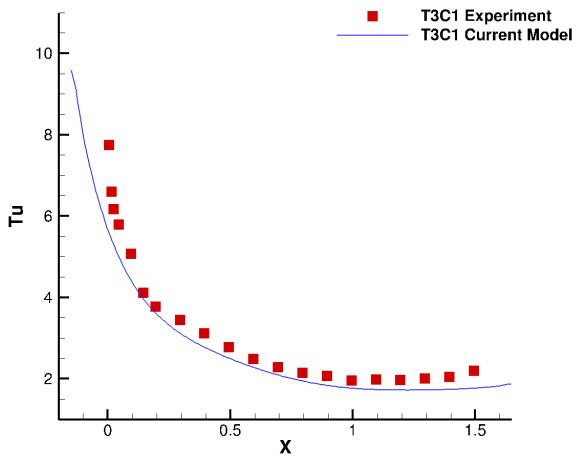


(b) Turbulence intensity decay in T3C1 case.

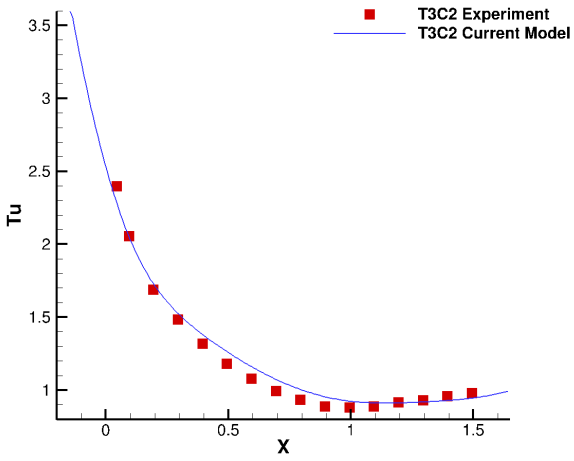


(c) Turbulence intensity decay in T3C2 case.

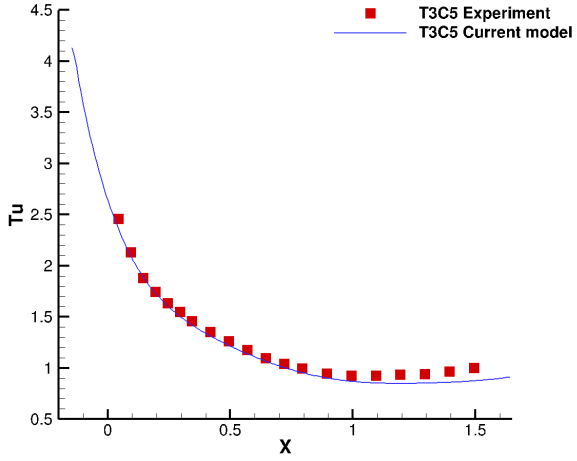


(d) Turbulence intensity decay in T3C5 case.

Figure 3.4 Free-stream velocity and turbulent intensity in T3C cases.

# CHAPTER 4. RESULTS AND DISCUSSION

## 4.1 Introduction

In this chapter, the skin friction coefficient $C_f$ in T3 series of flat plate test cases is calculated from the simulation data to present the ability of the current model to predict bypass transition. $C_f$ curves are plotted versus $x$-coordinate based Reynolds number,

$$Re_x = \frac{U_{fs}x}{\nu} \tag{4.1}$$

where $U_{fs}$ is the local free stream velocity.

T3A and T3B cases have zero pressure gradient along the flow direction, while T3C cases have varying pressure gradient. Firstly, as mentioned in previous chapter, various inlet conditions (i.e. free-stream turbulent kinetic energy $k$ and specific dissipation rate $\omega$) can affect the transition location. It turns out that this model is able to simulate this effect. Secondly, after transition, the transition model is supposed to switch into fully turbulent model, which means the intermittency function should recover to unity in turbulent region. As the results, the agreement with the experimentally measured skin friction curve as well as the transition location is good.

## 4.2 Sensitivity to Inlet Conditions

Skin friction curves computed with the same inlet dissipation rate ($\omega_{in}$) and with varying turbulent intensity are shown in figure (4.1.a). Note that $k \propto Tu^2$, with other conditions unchanged, the greater the intensity, the greater the kinetic energy. As we can see from the figure, increasing $Tu$ accelerates transition.

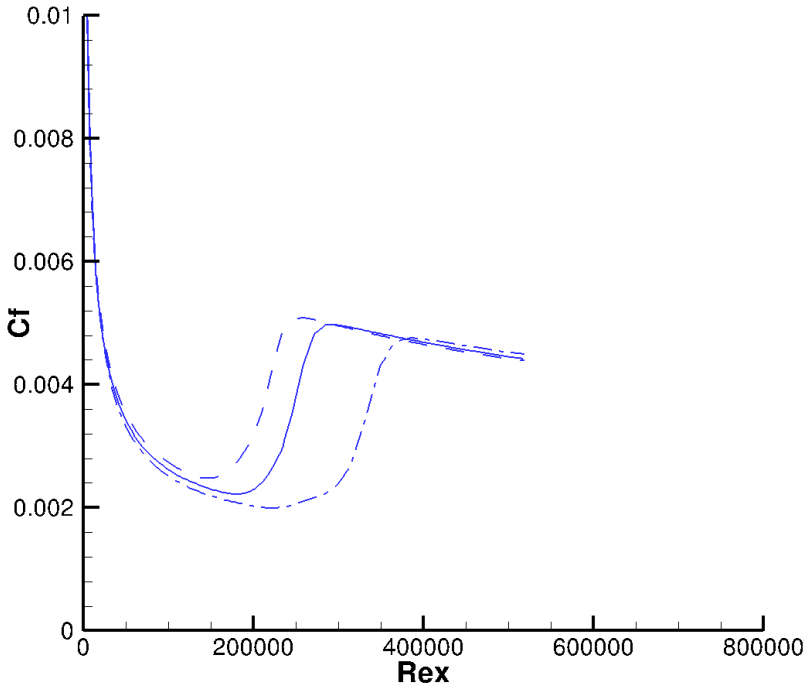


(a) $C_f$ curves for $Tu$=3.0 (dash-dot), $Tu$=3.5 (solid), $Tu$=4.0 (dash).

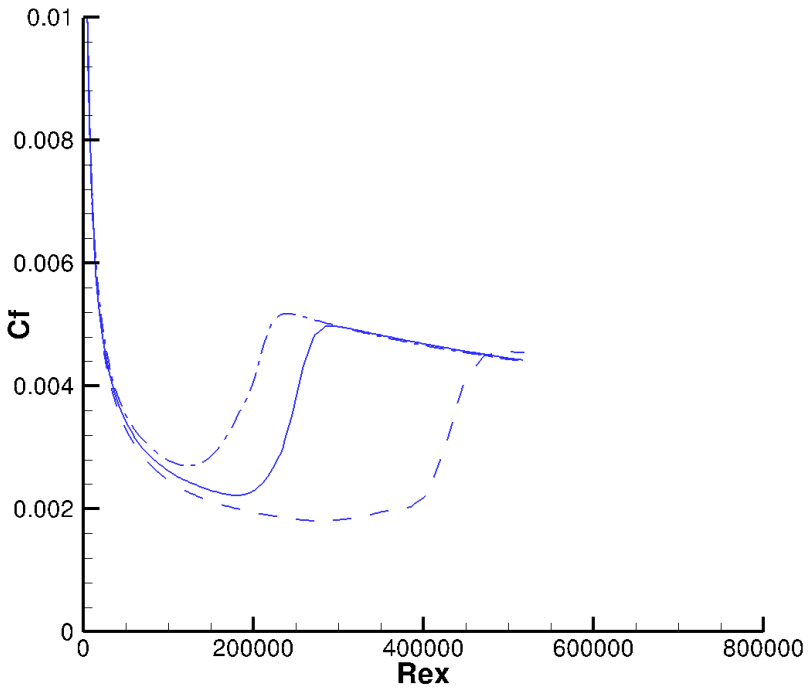


(b) $C_f$ curves for proper $\omega_{in}$ times 0.5 (dash-dot), proper $\omega_{in}$ (solid), proper $\omega_{in}$ times 2 (dash).

Figure 4.1 Sensitivity to inlet $k$ and $\omega$ (test case: T3A).

Skin friction curves computed with the same $Tu = 3.5\%$ and with different $\omega_{in}$ are displayed in (4.1.b). Decreasing $\omega_{in}$ makes turbulent energy decay slower and increases the eddy viscosity in free stream. Both effects accelerate transition, and vice versa.

## 4.3 Results for 2D Flat Plate Cases

### 4.3.1 Zero Pressure Gradient Cases

The contour of intermittency function, $\gamma$ on wall for zero pressure gradient cases are displayed in figure (4.2.b) and figure (4.3.b) for T3A and T3B cases respectively. The inlet condition for $\gamma$ is uniform with the value of unity, which is illustrated by the very narrow region with high value of $\gamma$ at the leading edge in the figures. Due to the effect of the sink term, $\gamma$ rapidly decreases to zero near wall right after the leading edge. With the diffusion of $\gamma$ from high value inside the free-stream to low value within the laminar boundary layer, transition is initiated, and hence the sink term starts to vanish with the source term switching on. At around the transition location, $\gamma$ increases to one and the boundary layer becomes turbulence. Figure (4.2.c) and (4.3.c) present the contour of turbulent kinetic energy $k$. At the transition region, $k$ starts to grow from zero and reaches the turbulent level when transition completes.

The computed skin friction coefficient for T3A case compared with the experimental data is displayed in figure (4.2.a). Blasius laminar boundary layer solution and half-empirical turbulent boundary layer solution are also plotted. The simulation result is in decent agreement with the measured data. The laminar region is slightly above the data and the transition part of the curve is a little sharper than the data. On the words, the onset location of transition is a bit late and the transition length is therefore short to reach the fully turbulent region on time. This issue exists in all the following cases.

The computed skin friction coefficient for T3B case compared with the experimental data is displayed in figure (4.3.a). Due to the high turbulence intensity, the skin friction before the completion of transition is over-predicted. But it does make an obvious improvement compared with results in Langtry and Menter (2009). The minimum skin friction obtained by the current model is close to 0.004 while results of other models are just around 0.005.

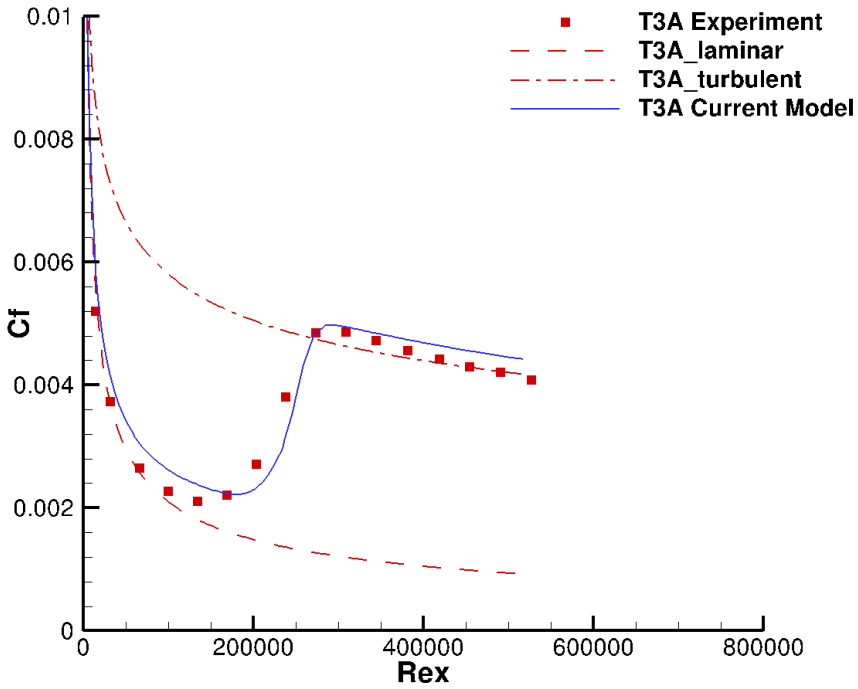


(a) Skin friction for T3A case.

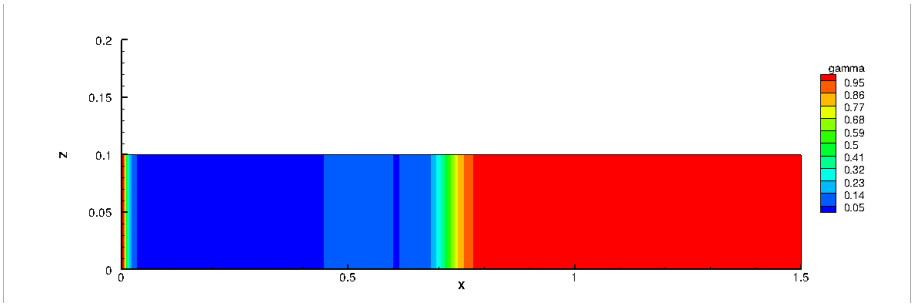


(b) Contour of $\gamma$ on wall, T3A.

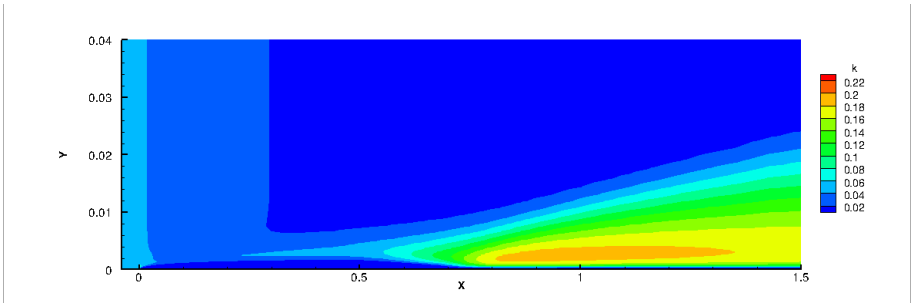


(c) Contour of $k$ with zoom in the boundary layer, T3A.

Figure 4.2 Simulation results for T3A.

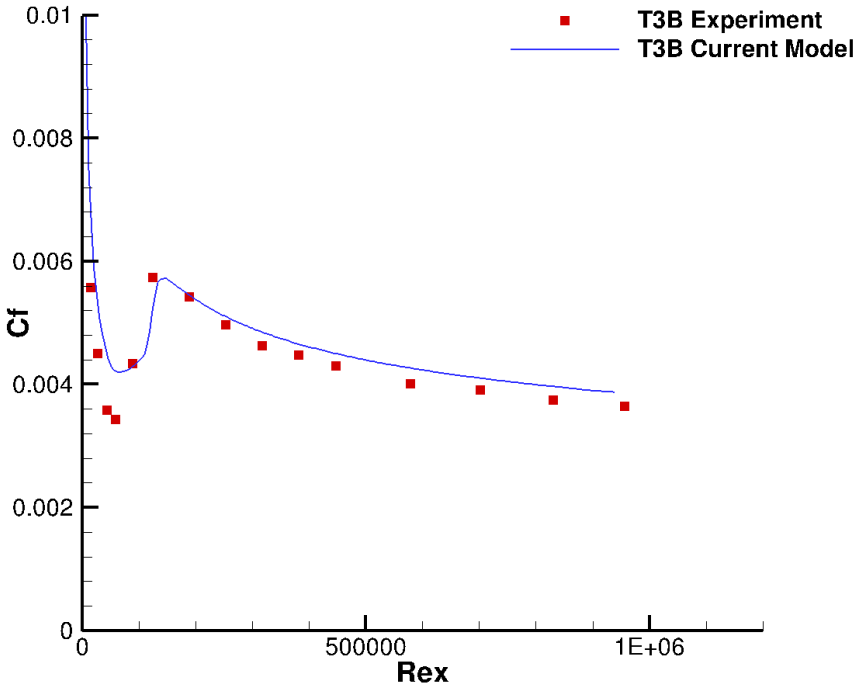


(a) Skin friction for T3B case.

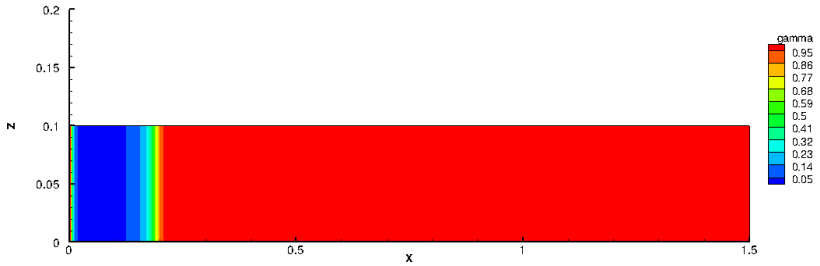


(b) Contour of $\gamma$ on wall, T3B.

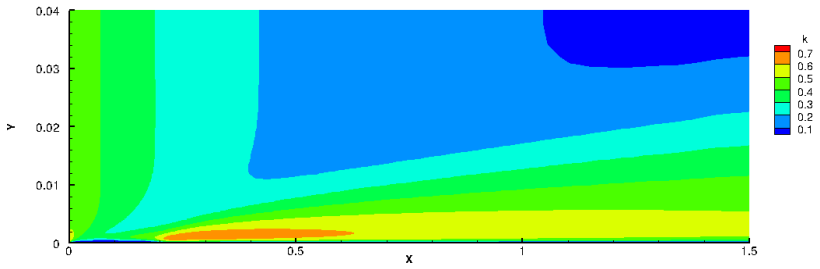


(c) Contour of $k$ with zoom in the boundary layer, T3B.

Figure 4.3 Simulation results for T3B.

### 4.3.2 Varying Pressure Gradient Cases

The T3C test cases can be classified into two groups. T3C1 is a high free-stream turbulence level case (first date point with $Tu \approx 8.0\%$), and the other T3C cases are moderate free-stream turbulence level cases (first data point with $Tu \approx 2.5\%$).

As for the T3B case, a high turbulence intensity case as well, the results shown in figure (4.4.a) for T3C1 are also better than those of others (Suluksna et al. (2009)). The smallest skin friction is closer to the experimental data. The mean velocity profile at the location of the highlight data point in figure (4.4.a) for this case is depicted in figure (4.4.b). The solid curve has acceptable agreement with the measured data.

The results for T3C2 case are shown in figure (4.5.a). In this case, the transition occurs in the adverse pressure gradient region because of the low Reynolds number. The onset location of transition is a bit late. But as mentioned above, the fast transition make it up and meet the turbulent region at almost the same Reynolds number as the measured data. But in figure (4.5.b), the mean velocity profile is over-predicted. It is induced by the under-prediction of the wall shear or the skin friction at that location. As the absolute value of the computed skin friction is relative low (0.002), an error of about 0.0015 would make a big difference to the skin velocity $u^*$ and hence $u^+$.

Figure (4.6.a) presents the skin friction coefficient computed by the current model for the T3C5 case. Transition occurs before the throat of the flow channel, i.e. within the favorable pressure gradient region since the inlet velocity and therefore the Reynolds number is high. Because of the strong favorable pressure gradient the transition length is extended to some extent. This model approximately predicts the behavior in broad agreement with the experiment. The mean velocity profile in the transition region shown in figure (4.6.b) is slightly under-predicted compared with the experimental data.

From figure (4.7) to (4.9), contours of $\gamma$ on wall and $k$ inside the domain for T3C cases are shown to illustrate the distribution of the $\gamma$ and its effect on the production of $k$, which is suppressed till $\gamma$ increases to full value.

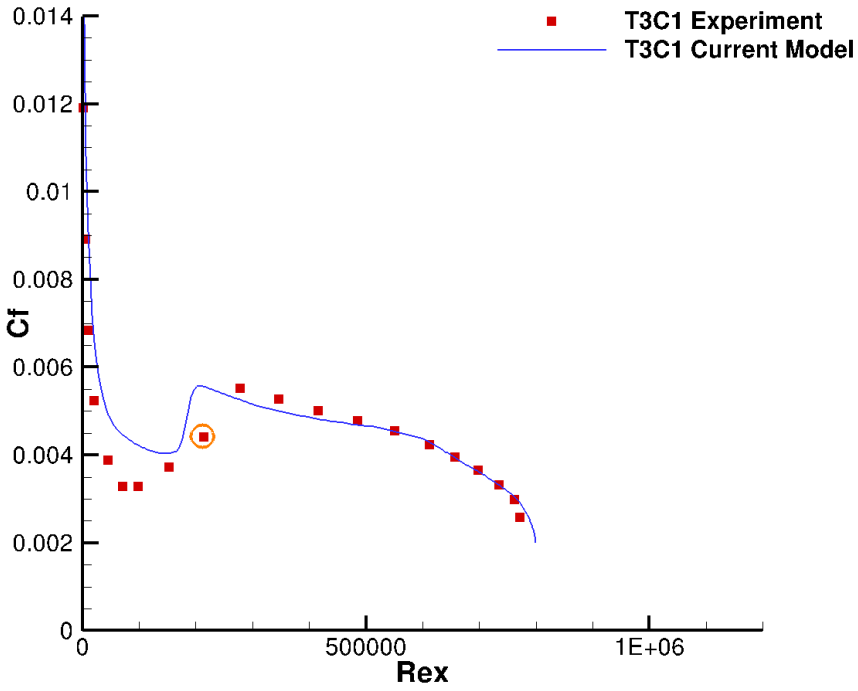


(a) $C_f$ curve for T3C1 case.

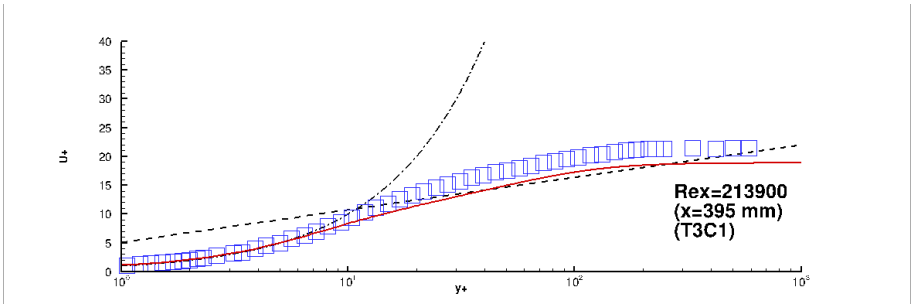


(b) $u^+$ vs. $y^+$ at the location of the data point highlighted in (a) for T3C1 case. Experimental data (square symbol), predicted result (solid), $u^+ = y^+$ (dash-dot), $u^+ = ln(y^+)/\kappa + B$ (dash, $\kappa$=0.41, $B$=5.1).

Figure 4.4 Plots of skin friction and velocity profile for T3C1.

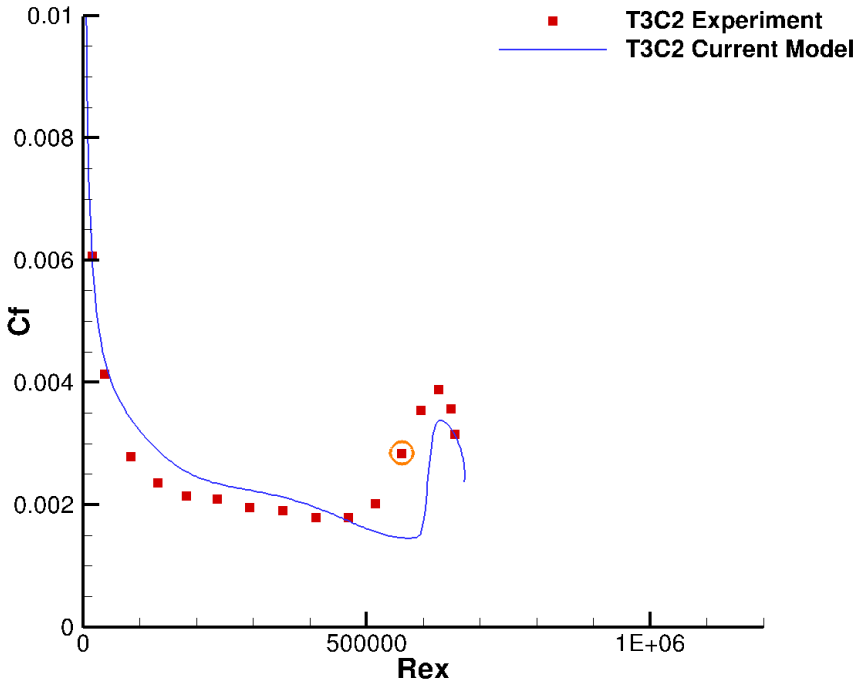


(a) $C_f$ curve for T3C2 case.

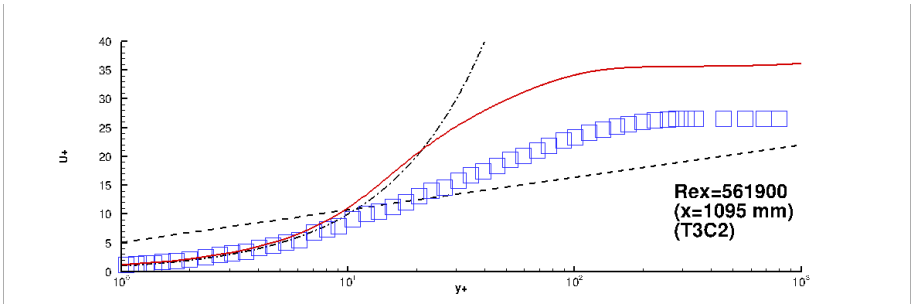


(b) $u^+$ vs. $y^+$ at the location of the data point highlighted in (a) for T3C2 case. Experimental data (square symbol), predicted result (solid), $u^+ = y^+$ (dash-dot), $u^+ = ln(y^+)/\kappa + B$ (dash, $\kappa$=0.41, $B$=5.1).

Figure 4.5 Plots of skin friction and velocity profile for T3C2.

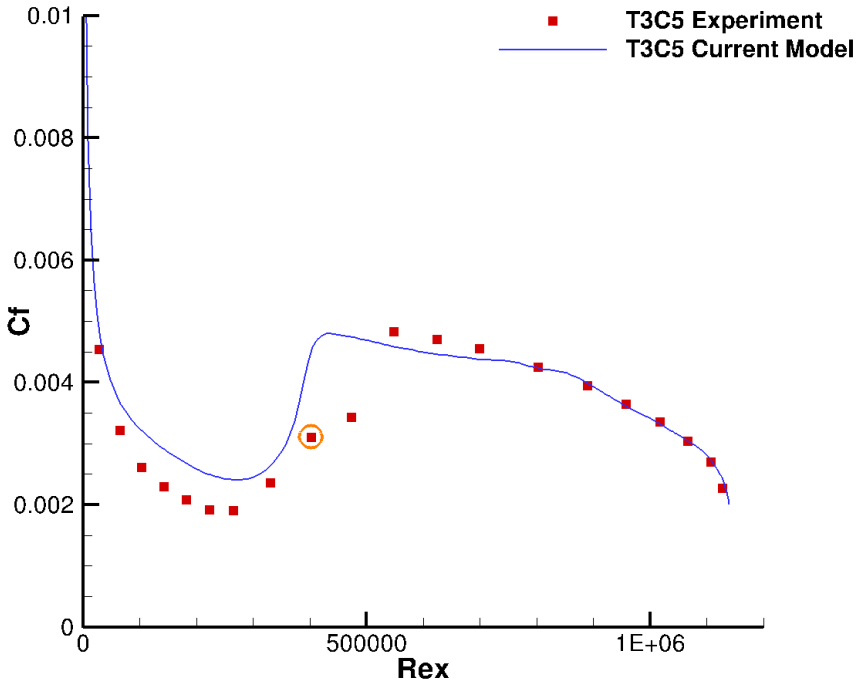


(a) $C_f$ curve for T3C5 case.

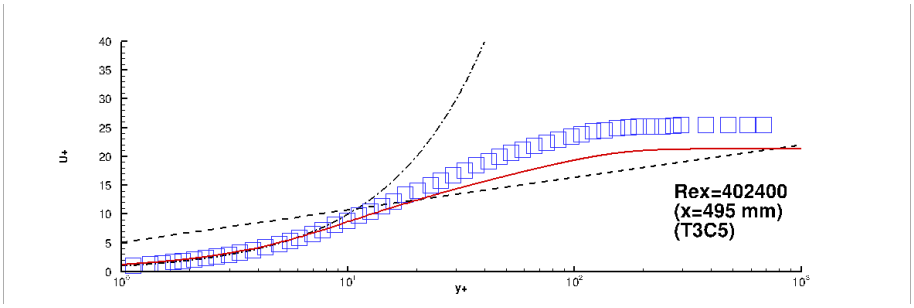


(b) $u^+$ vs. $y^+$ at the location of the data point highlighted in (a) for T3C5 case. Experimental data (square symbol), predicted result (solid), $u^+ = y^+$ (dash-dot), $u^+ = ln(y^+)/\kappa + B$ (dash, $\kappa$=0.41, $B$=5.1).

Figure 4.6 Plots of skin friction and velocity profile for T3C5.

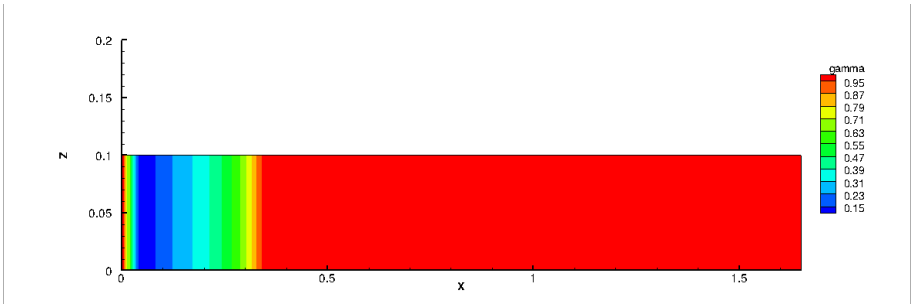


(a) Contour of $\gamma$ on wall, T3C1.

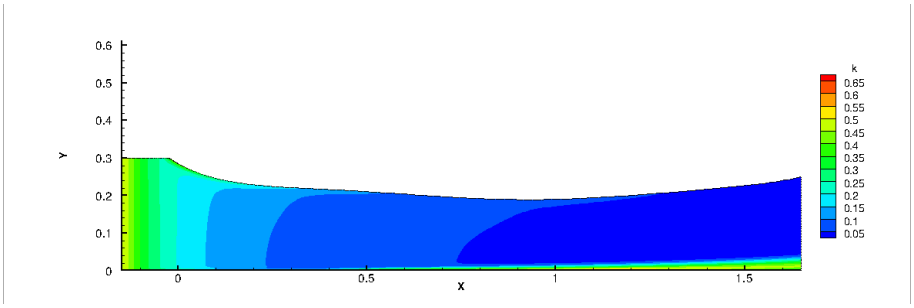


(b) Contour of $k$ from global view, T3C1.

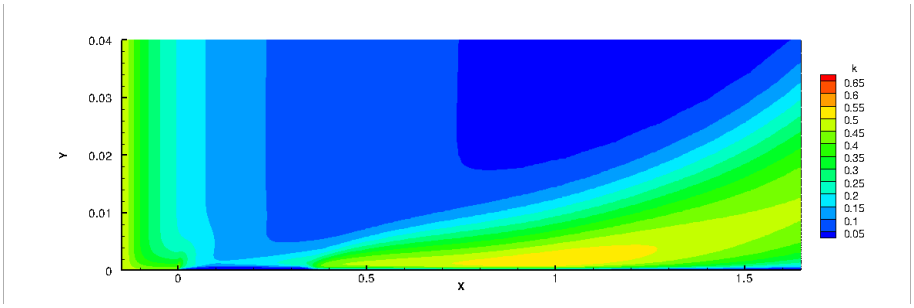


(c) Contour of $k$, zoom in the boundary layer, T3C1.

Figure 4.7 Contours of intermittency and kinetic energy for T3C1.

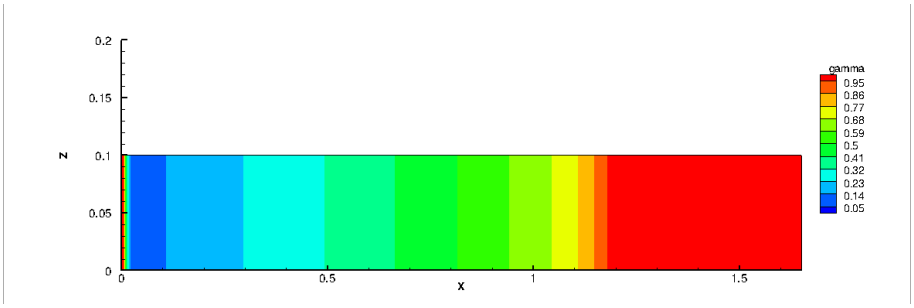


(a) Contour of $\gamma$ on wall, T3C2.

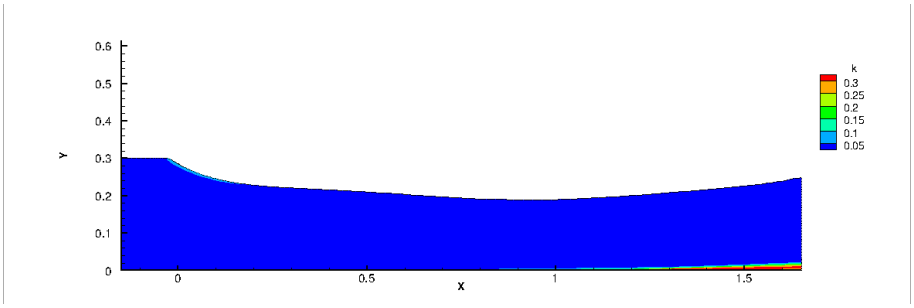


(b) Contour of $k$ from global view, T3C2.

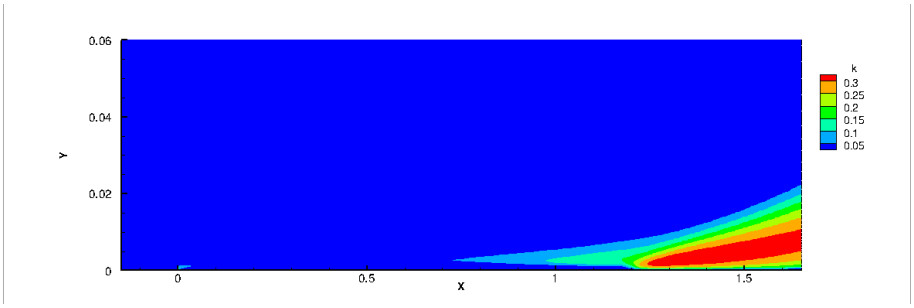


(c) Contour of $k$, zoom in the boundary layer, T3C2.

Figure 4.8 Contours of intermittency and kinetic energy for T3C2.

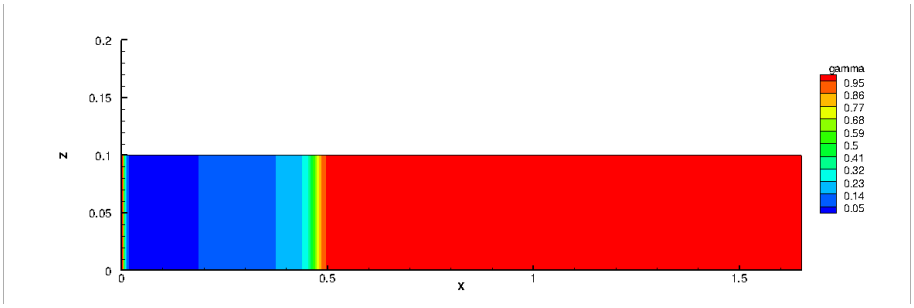


(a) Contour of $\gamma$ on wall, T3C5.

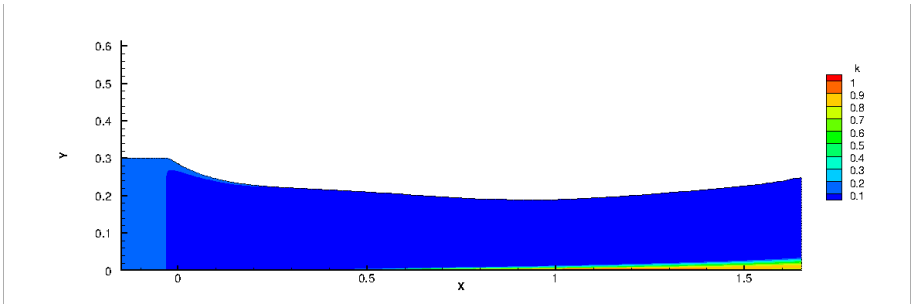


(b) Contour of $k$ from global view, T3C5.

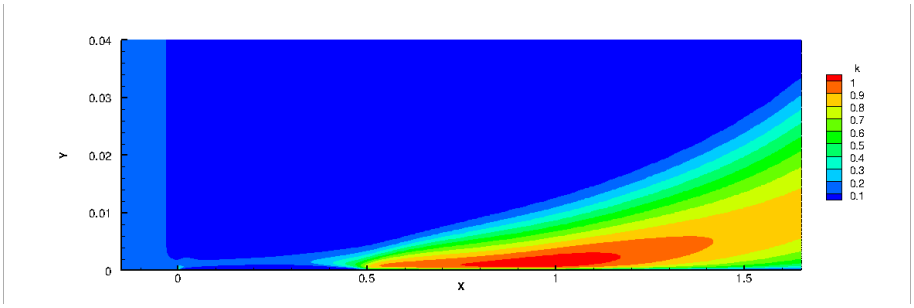


(c) Contour of $k$, zoom in the boundary layer, T3C5.

Figure 4.9 Contours of intermittency and kinetic energy for T3C5.

# CHAPTER 5. CONCLUSION

The objective of the present work is to propose an intermittency transition model that is simpler than those published and without data correlation. Although it remains quite empirical, the number of parameters is fewer and the role of each is more apparent. Moreover, this model can be compatible with general computational fluid dynamics techniques such as unstructured grids. Such a model has been developed and implemented in OpenFOAM, an open source CFD codes. It does not depend directly on pressure gradient (note that turbulence closures generally do not depend on pressure gradient explicitly.)

Only bypass transition in attached flow is taken into consideration in the body of this thesis. Langtry (2006) provides a form of modification for separated flow transition in their model in which a criterion of separation is invoked. The further work is to find another criterion of separation with accessible variables in the current model so that it is able to capture the separation and promote transition over that region. See some primary work in APPENDIX. After doing this, the model may be useful to more realistic problems in everyday industrial CFD simulations.

# . SEPARATION INDUCED TRANSITION

As mentioned in the first chapter, when a laminar boundary layer approaches to separation, inflection point instability becomes a cause to transition. In this mechanism, an instability wave serves as the precursor to transition, and the phenomenology is different from bypass transition, whose precursor is diffusion of free-stream turbulence into boundary layer.

The work for separation flow transition is still incomplete. Here is just the introduction of the idea and very preliminary results for this part of work. More research remains to be done on it in the future.

## Modification of the Model

Langtry (2006) points out that when separated flow transition is involved, their transition model without modification in terms of separation will predict the turbulent reattachment location too far downstream. Experimental results show that the lower the free-stream turbulence intensity is, the worse the agreement with the data will be. The low turbulent kinetic energy $k$ in the separating shear layer is attributed to the deficiency of the model because $k$ grows too slowly to cause the boundary layer to be turbulent and reattach on time.

The main idea which is used to modify the model for separation flow is to allow intermittency function to exceed 1 wherever the laminar boundary layer separates. This will lead to large production of $k$ and hence allow $k$ to grow rapidly to accelerate the transition or reattachment.

Learning from the idea described above, a criterion to locate the laminar separation should be introduced. It is known that the starting point of separation is where $\partial_y U|_{y=0}$ ($y$ represents the normal coordinate to the wall). And there would be an inflection point on the velocity profile. At this point, $\partial_y U$ is maximum and $\partial_y^2 U$ is zero. Above it, $\partial_y U$ decreases and $\partial_y^2 U$

becomes negative. Basically, once there is an inflection point on the velocity profile, $\partial_y^2 U$ will have non-negative values between the wall and the inflection point. Based on this fact, a criterion is selected as follows,

$$\sqrt{k}\tau^2 \mathbf{n}_w \cdot \nabla |S| > 0,$$

where the time scale $\tau$ is defined as,

$$\begin{cases} \tau_1 = \dfrac{1}{C_\mu \omega} \\ \tau_2 = 6.0\sqrt{\dfrac{\nu}{C_\mu k \omega}} \\ \tau_3 = \left(\tau_1^{C_\tau} \tau_2\right)^{\frac{1}{1+C_\tau}} \\ \tau = \max(\tau_1, \tau_3) \end{cases} \tag{A.1}$$

with $C_\tau = 1.625$ to get $T \propto y$ near the wall (Arolla and Durbin (2013)). $\mathbf{n}_w$ is the unit wall normal vector.

The separation modification is applied via using $\gamma_{eff}$,

$$\gamma_{eff} = \max\left\{\gamma, \min\left[100 \max\left(0, \sqrt{k}\tau^2 \mathbf{n}_w \cdot \nabla |S| - 0.0\right) \times F_{reattach}, 2.0\right]\right\} \tag{A.2}$$

where

$$F_{reattach} = e^{-\left(\frac{R_\nu R_t}{20}\right)^{1.2}}. \tag{A.3}$$

$\gamma_{eff}$ is used to replace $\gamma$ in the production term of $k$ equation while $\gamma$ equation itself does not change. After the $\gamma$ equation converges to a solution, $\gamma_{eff}$ will be calculated and come into play to compute $k$. $F_{reattach}$ works like $F_{turb}$ in sink term, which disables the modification outside the boundary layer and the viscous sublayer.

## Case Test

Another flat plate test case, T3C3, in T3C series is selected. See the inlet conditions for this case in table (A.1). They are specified as such that the free-stream velocity and turbulence decay along flow direction would agree with the experimental data. Note that it is not really a separation case though the Reynolds number is low and the minimum skin friction is close to zero. However, the model without the separation modification would produce separation region and have skin friction below zero. The reason has been explained above. Diffusion of the low free-stream turbulence intensity cannot cancel the effect of the sink term so that the laminar boundary layer separates along with the effect of adverse pressure gradient. After the production of $k$ forced to be high via the effect of $\gamma_{eff}$, the $C_f$ curve for T3C3 case is improved significantly. See figure (A.1).

Table A.1 Inlet condition for T3C3 case

| **Case** | $U_{in}$**(m/s)** | $Tu_{in}$**(%)** | $R_t$ |
|---|---|---|---|
| T3C3 | 3.8 | 3.4 | 8 |

This modification is devised as such that a negligible effect should be involved on the general attached flow cases. The new model has been used to compute the T3C5 case and the $C_f$ curves for both the models before and after modification are shown in figure (A.2). As expected, the difference can be neglected.

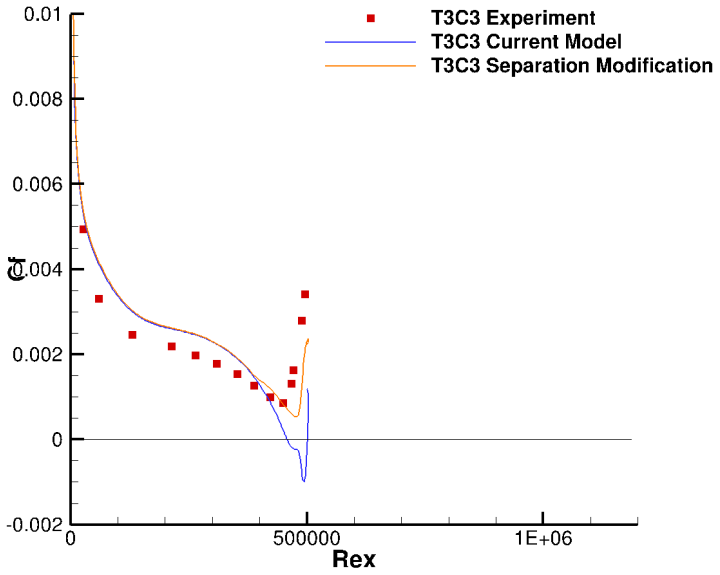


Figure A.1 The effect of the separation modification for T3C3 case.

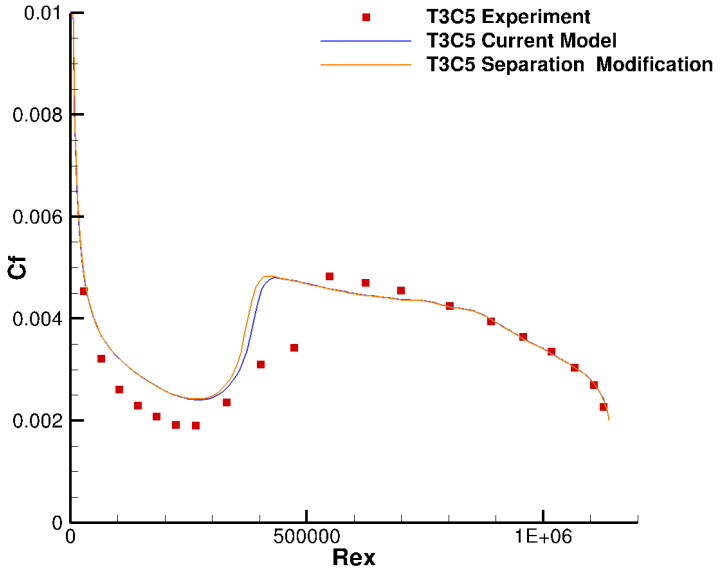


Figure A.2 The effect of the separation modification for T3C5 case.

# BIBLIOGRAPHY

Abu-Gannam, B. J. and Shaw, R. (1980). Natural transition of boundary layers- the effect of turbulence, pressure gradient and flow history. *Journal of Mechanical Engineering Science*, *22*, 213–228.

Arolla, S. K. and Durbin P. A. (2013). Modeling rotation and curvature effects with scalar eddy viscousity model framework. *International Journal of Heat and Fluid Flow*, *39*, 78-89.

Durbin, P.A. (2011). *Statistical theory and modeling for turbulent flows*. United Kingtdom: John Wiley & Sons, Ltd.

Durbin, P. A. (2012). An intermittency model for bypass transition. *International Journal of Heat and Fluid Flow*, *36*, 1-6.

Langtry, R. B. (2006). *A correlation-based transition model using local variables for unstructured parallelized CFD codes*. Ph.D. Thesis, University of Stuttgart, Stuttgart, Germany

Langtry, R. B. and Menter, F. R. (2009). Correlation-based transition modeling for unstructured parallelized computational fluid dynamics codes. *AIAA Journal*, *47*(12), 2894–2906.

Praisner, T. J. and Clark, J. P. (2007). Predicting transition in turbomachinery- part I: A review and new model development. *Journal of Turbomachinery*, *129*, 1-13.

Suluksna, K., Dechaumphai, P. and Juntasaro, E. (2009). Correlation for modeling transitional boundary layers under influences of free stream turbulence and pressure gradient. *International Journal of Heat and Fluid Flow*, *30*, 66-72.

Walters, D. K and Cokaljat, D. (2008). A three-equation eddy-viscosity model for Renolds-averaged Navier-Stokes simulations of transition flow. *Journal of Fluids Engineering*, *130*(121401).

Wilcox, D. C. (1993). *Turbulence Modeling for CFD*. DCW Industries.

Zaki, T. and Durbin, P. A. (2005). Mode interaction and the bypass route to transition. *Journal of Fluid Mechanics*, *531*, 85-111.